UNIVERSIDAD DE CONCEPCIÓN

Centro de Investigación en Ingeniería Matemática (CI^{2}MA)

An HHO formulation for a Neumann problem on general meshes

Rommel Bustinza, Jonathan Munguia

PREPRINT 2019-06

SERIE DE PRE-PUBLICACIONES

An HHO formulation for a Neumann problem on general meshes

ROMMEL BUSTINZA* and JONATHAN MUNGUIA LA COTERA†

Abstract

In this work, we study a Hybrid High-Oder (HHO) method for an elliptic diffusion problem with Neumann boundary condition. The proposed method has several features, such as: i) the support of arbitrary approximation order polynomial at mesh elements and faces on general polyhedral meshes, ii) the design of a local (element-wise) discrete gradient reconstruction operator and a local stabilization term, that weakly enforces the matching between local element- and face- based on degrees of Freedom (DOF), and iii) cheap computational cost, thanks to static condensation and compact stencil. We prove the well-posedness of our HHO formulation, and obtain the optimal error estimates, according to [9]. Implementation aspects are throughly discussed. Finally, some numerical examples are provided, which are in agreement with our theoretical results.

Keywords: Neumann problem, Diffusion, General Meshes, High-Order, Gradient Reconstruction.

1 Introduction

The approximation of diffusive problems on general polyhedral meshes have received an increasing attention over the last few years, motivated in particular by applications in the geosciences, where the mesh is often adapted to geological layers, cracks and faults leading to cells with polyhedral shape and to non-matching interfaces. These considerations are included in the context of Hybrid High-Order methods (HHO). The HHO method is derived in terms of a primal formulation, and is designed from two key ingredients:

i) a potential reconstruction in each mesh cell, and

ii) a face-based stabilization consistent, with the high-order provided by the reconstruction.

*Departamento de Ingeniería Matemática & Centro de Investigación en Ingeniería Matemática (CI^{2}MA), Universidad de Concepción, Casilla 160-C, Concepción, Chile, e-mail: rbustinz@ing-mat.udec.cl

†Instituto de Matemática y Ciencias Afines (IMCA), Calle Los Biólogos 245, Urb. San César, Primera Etapa, La Molina, Lima & Escuela Profesional de Matemática, Facultad de Ciencias, Universidad Nacional de Ingeniería, Av. Túpac Amaru 210 (Puerta No. 5), Rímac, Casilla 31-139, Lima, Perú, e-mail: munguia.la.cotera@gmail.com

This design relies on intermediate cell-based discrete unknowns, in addition to the face-based ones (hence, the term hybrid). We remark that the cell-based unknowns can be eliminated by static condensation, as it has already been pointed out in [8], [11].
As low-order methods on polyhedral meshes have been studied for quite some time, we mention that HHO can be seen as a Finite Volume method (FVM) (cf. [13], [15]) for polynomial of order $k = 0$ (see Section 2.5 in [8]). We can also express the HHO method into an equivalent mixed formulation (cf. [12], [10]). This equivalent formulation allows us to identify a conservative numerical trace for the flux, and thus HHO methods can be seen as a generalization of HDG methods (cf. [4]). Moreover, in Section 2.4 in [4], we find a link between a non-conforming Virtual Element Method considered in [1], and HHO methods, by defining an isomorphism between the HHO degrees of freedom and a local virtual finite-dimensional space (containing those polynomial functions leading to optimal approximation properties), we identify the projection operator related to the elliptic operator of HHO.

In what follows, we describe the model problem. Let $\Omega \subset \mathbb{R}^d$, $d \in \{2, 3\}$, be an open, bounded, polytopic domain with Lipschitz-continuous boundary $\Gamma := \partial\Omega$ and unit outward normal $\boldsymbol{n}$. Let $K \in [L^\infty(\Omega)]^{d\times d}$ be a bounded, measurable, and symmetric tensor describing the material properties, $f \in L^2(\Omega)$ is the forcing term and $g \in L^2(\Gamma)$ is the flux through the boundary. We focus on the following variable-diffusion problem with Neumann boundary condition:

$$-\nabla \cdot (K\nabla u) = f \text{ in } \Omega\,, \tag{1a}$$

$$K\nabla u \cdot \boldsymbol{n} = g \text{ on } \Gamma\,. \tag{1b}$$

It is well known that the data f and g must satisfy the compatibility condition

$$\int_\Omega f + \int_\Gamma g = 0\,. \tag{2}$$

From here on, we assume that K is strongly elliptic, that is there exist two positive constants c_1 and c_2 such that

$$c_1|\boldsymbol{\xi}|^2 \leq \boldsymbol{\xi}^T\, K(x)\, \boldsymbol{\xi} \leq c_2|\boldsymbol{\xi}|^2 \quad \forall \boldsymbol{\xi} \in \mathbb{R}^d,\, \forall x \in \Omega,$$

where $|\cdot|$ represents the usual Euclidean norm. The strong ellipticity implies that matrix $K(x)$ is uniformly positive definite and thus non-singular for every $x \in \Omega$.

For any connected subset $X \subset \bar{\Omega}$ with nonzero Lebesgue measure, the inner product and norm of the Lebesgue space $L^2(X)$ are denoted by $(\cdot,\cdot)_X$ and $||\cdot||_X$, respectively. Similar notations will be used for $L^2(X)^d$ and $L^2(\Gamma)$. It is not difficult to deduce that the weak formulation of (1) reads as: *Given $f \in L^2(\Omega)$ and $g \in L^2(\Gamma)$, we seek $u \in U := \{v \in H^1(\Omega) : (v, 1)_\Omega = 0\}$ such that*

$$(K\nabla u, \nabla v)_\Omega = (f, v)_\Omega + (g, v)_\Gamma \quad \forall v \in U. \tag{3}$$

In addition, thanks to the Poincaré-Wintinger inequality and the Lax-Milgram lemma, we can ensure that the problem (3) is well-posed.

We can mention that HHO for Dirichlet conditions have been treated in [9], and for mixed conditions in [12]. Then, the focus of the present work is to describe the Hybrid High-Order method for variable-diffusion problems with Neumann boundary conditions. It is important to

emphasize that the involved analysis is not contained in the context of [12].
In Section 2, we introduce the model problem, our main analysis tools, the Degrees of Freedom (DOFs) in the context of HHO method, and the potential reconstruction operator, with its key properties. In Section 3, we introduce the discrete problem and study its stability. In Section 4, we perform the error analysis, first in the energy-norm and then in the L^2-norm under additional elliptic regularity assumption. In Section 5, we discuss the computational implementation and, finally in Section 6, we present some numerical results, which are in agreement with our theoretical results.

2 Discrete settings

Let $\mathcal{H} \subset \mathbb{R}^+$ denote a countable set of meshsizes having 0 as its unique accumulation point and $(\mathcal{T}_h)_{h\in\mathcal{H}}$ a h-refined admissible mesh sequence of $\overline{\Omega}$ (see Section 1.4 in [7]). Each mesh $\mathcal{T}_h$ of this sequence is a finite collection T of nonempty, disjoint, open, polytopic elements such that $\overline{\Omega} = \bigcup_{T\in\mathcal{T}_h} \overline{T}$ and $h = \max_{T\in\mathcal{T}_h} h_T$ (with h_T the diameter of T), and there is a matching simplicial submesh of $\mathcal{T}_h$ with locally equivalent mesh size and which is shape-regular in the usual sense (γ is the mesh regularity parameter). We call a face any hyperplanar closed connected subset F of $\overline{\Omega}$ with positive $(d-1)$-dimensional measure and such that (i) either there exist $T_1, T_2 \in \mathcal{T}_h$ such that $F \subset \partial T_1 \cap \partial T_2$ (F is called an interior face) or (ii) there exists $T \in \mathcal{T}_h$ such that $F \subset \partial T \cap \partial\Omega$ (F is called a boundary face). Interior faces are collected in the set $\mathcal{F}_h^i$, boundary faces in $\mathcal{F}_h^\partial$, and we set $\mathcal{F}_h := \mathcal{F}_h^i \cup \mathcal{F}_h^\partial$. The diameter of a face $F \in \mathcal{F}_h$ is denoted by h_F. For each $T \in \mathcal{T}_h$, $\mathcal{F}_T := \{F \in \mathcal{F}_h \,|\, F \subset \partial T\}$ defines the set of faces lying on the boundary of T and, for each $F \in \mathcal{F}_T$, $\boldsymbol{n}_{TF}$ is the unit normal to F pointing out of T. In an admissible mesh sequence, for any $T \in \mathcal{T}_h$, and any $F \in \mathcal{F}_T$, h_F is uniformly comparable to h_T in the sense that

$$\gamma^2 h_T \leq h_F \leq h_T, \tag{4}$$

and the card($\mathcal{F}_T$) is uniformly bounded. The usual discrete and multiplicative trace inequalities hold on element faces. The following assumptions and notations will be taken into account in this work:

1. There is a partition P_Ω of Ω so that K is piecewise Lipschitz, and the mesh $\mathcal{T}_h$ fits the (polytopal) partition P_Ω associated with the diffusion tensor K in the sense that, there is a unique Ω_i in P_Ω containing T. For simplicity of exposition, we assume that K is a piecewise polynomial.

2. We denote by $\underline{K}_T$ and $\overline{K}_T$ the lowest and largest eigenvalues of K in T. We introduce the local heterogeneity/anisotropy ratio $\rho_T := \overline{K}_T/\underline{K}_T \geq 1$.

3. Furthermore, $A \lesssim B$ denotes the inequality $A \leq CB$ with positive constant C independent of the polynomial degree k, the meshsize h and the diffusion tensor K.

4. To avoid the proliferation of symbols, we assume that for all $T \in \mathcal{T}_h$, the Lipschitz constant of K in T, say L_T^k, satisfies $L_T^k \lesssim \overline{K}_T$.

In the following lemma, we show that the L^2-orthogonal projector onto polynomial spaces have optimal approximation properties on each mesh element.

Lemma 2.1 (Approximation property of Orthogonal projector) . *Given an integer $l \geq 0$, and $T \in \mathcal{T}_h$, we denote by π_T^l the L^2-orthogonal projector onto $\mathbb{P}_d^l(T)$. Then, for any $s, t \in \mathbb{R}$ with $0 \leq s \leq t \leq l+1$ there exists $C_{app} = C_{app}(\gamma, l) > 0$, such that*

$$|v - \pi_T^l v|_{H^s(T)} \leq C_{app} h_T^{t-s} |v|_{H^t(T)}, \quad \forall\, v \in H^t(T). \tag{5}$$

Besides, there exists $C'_{app} > 0$ such that, for all t, $1/2 < t \leq l+1$, there holds

$$\|v - \pi_T^l v\|_{\partial T} \leq C'_{app} h_T^{t-1/2} |v|_{H^t(T)}, \quad \forall\, v \in H^t(T), \tag{6}$$

where $|\cdot|_{H^t(T)}$ and $|\cdot|_{H^s(T)}$ denotes the corresponding seminorms on Sobolev spaces $H^t(T)$ and $H^s(T)$, respectively.

Proof. We refer to Theorems 3.2 and 3.3 in [17]. □

2.1 Degrees of freedom (DOFs)

Let a polynomial degree $k \geq 0$ be fixed. For all $T \in \mathcal{T}_h$, we define the local space of DOFs as $\underline{\boldsymbol{U}}_T^k := \mathbb{P}_d^k(T) \times \left\{ \bigtimes_{F \in \mathcal{F}_T} \mathbb{P}_{d-1}^k(F) \right\}$, where $\mathbb{P}_d^k(T)$ (resp., $\mathbb{P}_{d-1}^k(F)$) is spanned by the restrictions to T (resp., F) of d-variate (resp., $(d-1)$-variate) polynomials of total degree $\leq k$. And the global space of DOFs on the domain Ω.

$$\underline{\boldsymbol{U}}_h^k := \left\{ \bigtimes_{T \in \mathcal{T}_h} \mathbb{P}_d^k(T) \right\} \times \left\{ \bigtimes_{F \in \mathcal{F}_h} \mathbb{P}_{d-1}^k(F) \right\}.$$

For all $T \in \mathcal{T}_h$, we define the local reduction operator $\underline{\mathrm{I}}_T^k : H^1(T) \to \underline{\boldsymbol{U}}_T^k$ such that, for all $v \in H^1(T)$,

$$\underline{\mathrm{I}}_T^k v := (\pi_T^k v, (\pi_F^k v)_{F \in \mathcal{F}_T}), \tag{7}$$

where π_T^k and π_F^k are the L^2-orthogonal projectors onto $\mathbb{P}_d^k(T)$ and $\mathbb{P}_{d-1}^k(F)$, respectively. The corresponding global interpolation operator $\underline{\mathrm{I}}_h^k : H^1(\Omega) \to \underline{\boldsymbol{U}}_h^k$ is such that, for all $v \in H^1(\Omega)$,

$$\underline{\mathrm{I}}_h^k v := ((\pi_T^k v)_{T \in \mathcal{T}_h}, (\pi_F^k v)_{F \in \mathcal{F}_h}). \tag{8}$$

2.2 Local Gradient reconstruction

For all $T \in \mathcal{T}_h$, and $l \geq 1$, $\mathbb{P}_d^{k+1,0}(T)$ denotes the space of d-variate polynomial functions of total degree $\leq l$, that have zero mean value on T. Then, we define the local gradient reconstruction operator $G_T^k : \underline{\boldsymbol{U}}_T^k \to \nabla \mathbb{P}_d^{k+1,0}(T)$ such that, for each $\underline{\boldsymbol{v}}_T := (v_T, (v_F)_{F \in \mathcal{F}_T}) \in \underline{\boldsymbol{U}}_T^k$ and each $w \in \mathbb{P}_d^{k+1,0}(T)$,

$$(K G_T^k \underline{\boldsymbol{v}}_T, \nabla w)_T = (K \nabla v_T, \nabla w)_T + \sum_{F \in \mathcal{F}_T} (v_F - v_T, K \nabla w \cdot \boldsymbol{n}_{TF})_F, \tag{9}$$

where we recall $\boldsymbol{n}_{TF}$ is the unit normal to F pointing out of T. Next, we define the potential reconstruction operator $p_T^k : \underline{\boldsymbol{U}}_T^k \to \mathbb{P}_d^{k+1}(T)$ such that, for all $\underline{\boldsymbol{v}}_T \in \underline{\boldsymbol{U}}_T^k$,

$$\nabla p_T^k \underline{\boldsymbol{v}}_T := G_T^k \underline{\boldsymbol{v}}_T, \qquad \int_T p_T^k \underline{\boldsymbol{v}}_T := \int_T v_T. \tag{10}$$

The following result shows that $p_T^k \underline{\mathrm{I}}_T^k$ is the K-weighted elliptic projector onto $\mathbb{P}_d^{k+1}(T)$.

Lemma 2.2 (Characterization of $p_T^k \underline{\mathrm{I}}_T^k$ and polynomial consistency) . *For every $v \in H^1(T)$ and $w \in \mathbb{P}_d^{k+1}(T)$, there holds*

$$(K\nabla(v - p_T^k \underline{\mathrm{I}}_T^k v), \nabla w)_T = ((K - \overline{K}_T), \nabla w)_T - \sum_{F \in \mathcal{F}_T} (\pi_F^k v - \pi_T^k v, (K - \overline{K}_T)\nabla w \cdot \boldsymbol{n}_{TF})_F, \quad (11)$$

where $\overline{K}_T$ denotes the mean-value of K on T. In addition, if K is piecewise constant, we obtain the following orthogonality property:

$$(K\nabla(v - p_T^k \underline{\mathrm{I}}_T^k v), \nabla w)_T = 0, \quad (12)$$

and the polynomial consistency:

$$p_T^k \underline{\mathrm{I}}_T^k v = v \quad \forall\, v \in \mathbb{P}_d^{k+1}(T). \quad (13)$$

Proof. We refer to Lemma 2.1 in [9] for (11) and Lemma 3.1 in [12] for (12) and (13). □

Lemma 2.3 (Approximation properties for $p_T^k \underline{\mathrm{I}}_T^k$) . *There exists a real number $C > 0$, depending of γ and d, but independent of the polynomial degree, the meshsize, and the diffusion tensor. So that for any $v \in H^s(T)$ there holds:*

$$\begin{aligned} &\left\| v - p_T^k \underline{\mathrm{I}}_T^k v \right\|_T + h_T^{1/2} \left\| v - p_T^k \underline{\mathrm{I}}_T^k v \right\|_{\partial T} \\ &\qquad + h_T \left\| \nabla(v - p_T^k \underline{\mathrm{I}}_T^k v) \right\|_T + h_T^{3/2} \left\| \nabla(v - p_T^k \underline{\mathrm{I}}_T^k v) \right\|_{\partial T} \leq C \rho_T^{\alpha} h_T^s \left\| v \right\|_{H^s(T)}, \end{aligned} \quad (14)$$

for all $s \in \{2, \cdots, k+2\}$. Here, $\alpha = 1/2$ if K is piecewise constant, and $\alpha = 1$ otherwise.

Proof. We refer to Lemma 2.1 in [9]. □

3 Formulation

Now, we define the discrete global space for our HHO formulation, as

$$\underline{\boldsymbol{U}}_h^{k,0} := \left\{ \underline{\boldsymbol{v}}_h \in \underline{\boldsymbol{U}}_h^k : (v_h, 1)_\Omega = 0 \right\},$$

with $v_h := \{v_T\}_{T \in \mathcal{T}_h}$, and the following discrete semi norm on $\underline{\boldsymbol{U}}_h^k$,

$$\|\underline{\boldsymbol{v}}_h\|_{K,h}^2 := \sum_{T \in \mathcal{T}_h} \rho_T^{-1} \|\underline{\boldsymbol{v}}_T\|_{K,T}^2, \quad \forall\, \underline{\boldsymbol{v}}_h \in \underline{\boldsymbol{U}}_h^k, \quad (15)$$

where $\|\underline{\boldsymbol{v}}_T\|_{K,T}^2 := \|K^{1/2}\nabla v_T\|_T^2 + |\underline{\boldsymbol{v}}_T|_{K,\partial T}^2$ and $|\underline{\boldsymbol{v}}_T|_{K,\partial T}^2 := \sum_{F \in \mathcal{F}_T} \dfrac{k_F}{h_F} \|v_F - v_T\|_F^2$, with $k_F := \|\boldsymbol{n}_{TF}^T K \boldsymbol{n}_{TF}\|_{L^\infty(F)}$, for all $\underline{\boldsymbol{v}}_T \in \underline{\boldsymbol{U}}_T^k$.

Proposition 3.1 (Norm $\|\cdot\|_{K,h}$) . *The map $\|\cdot\|_{K,h}$ defines a norm on $\underline{\boldsymbol{U}}_h^{k,0}$.*

Proof. It is enough to prove that $\forall \underline{\boldsymbol{v}}_h \in \underline{\boldsymbol{U}}_h^{k,0}$: $\|\underline{\boldsymbol{v}}_h\|_{K,h} = 0 \Rightarrow \underline{\boldsymbol{v}}_h = \underline{0}_h$. Let $\underline{\boldsymbol{v}}_h \in \underline{\boldsymbol{U}}_h^{k,0}$ be such that $\|\underline{\boldsymbol{v}}_h\|_{K,h} = 0$. By definition of $\|\cdot\|_{K,h}$, we obtain (cf. (15))

$$\nabla v_T \equiv 0 \quad \text{and} \quad v_T|_F = v_F \quad \forall F \in \mathcal{F}_T \ \forall T \in \mathcal{T}_h. \tag{16}$$

Then, from (16) we infer that v_h is piecewise constant on $\mathcal{T}_h$, and for each interior face $F \in \mathcal{F}_h$, there exist $T_1, T_2 \in \mathcal{T}_h$ with $F \subset \partial T_1 \cap \partial T_2$, such that $v_{T_1}|_F = v_F = v_{T_2}|_F$. This means that v_h is continuous on $\bar{\Omega}$, and thus an element in $\mathbb{P}_0(\bar{\Omega})$. Finally, due to the condition $(v_h, 1)_\Omega = 0$, we deduce that $v_h = 0$, and we conclude the proof. □

Hereafter, the local potential reconstruction $P_T^k : \underline{\boldsymbol{U}}_T^k \to \mathbb{P}_d^{k+1}(T)$ is defined such that, for all $\underline{\boldsymbol{v}}_T \in \underline{\boldsymbol{U}}_T^k$,

$$P_T^k \underline{\boldsymbol{v}}_T := v_T + (p_T^k \underline{\boldsymbol{v}}_T - \pi_T^k p_T^k \underline{\boldsymbol{v}}_T). \tag{17}$$

Now, to discretize the left-hand of (3), we introduce the following bilinear forms on $\underline{\boldsymbol{U}}_h^k \times \underline{\boldsymbol{U}}_h^k$:

$$a_h(\underline{\boldsymbol{u}}_h, \underline{\boldsymbol{v}}_h) = \sum_{T \in \mathcal{T}_h} a_T(\underline{\boldsymbol{u}}_T, \underline{\boldsymbol{v}}_T), \quad s_h(\underline{\boldsymbol{u}}_h, \underline{\boldsymbol{v}}_h) = \sum_{T \in \mathcal{T}_h} s_T(\underline{\boldsymbol{u}}_T, \underline{\boldsymbol{v}}_T), \tag{18}$$

where, for each $T \in \mathcal{T}_h$, the local bilinear forms a_T and s_T defined on $\underline{\boldsymbol{U}}_T^k \times \underline{\boldsymbol{U}}_T^k$, are given by

$$a_T(\underline{\boldsymbol{u}}_T, \underline{\boldsymbol{v}}_T) := (K G_T^k \underline{\boldsymbol{u}}_T, G_T^k \underline{\boldsymbol{v}}_T)_T + s_T(\underline{\boldsymbol{u}}_T, \underline{\boldsymbol{v}}_T), \tag{19a}$$

$$s_T(\underline{\boldsymbol{u}}_T, \underline{\boldsymbol{v}}_T) := \sum_{F \in \mathcal{F}_T} \frac{k_F}{h_F} (\pi_F^k(u_F - P_T^k \underline{\boldsymbol{u}}_T), \pi_F^k(v_F - P_T^k \underline{\boldsymbol{v}}_T))_F. \tag{19b}$$

The linear functional on the right hand side in (3) is discretized by means of the linear functional on $\underline{\boldsymbol{U}}_h^k$ such that

$$b_h(\underline{\boldsymbol{v}}_h) := \sum_{T \in \mathcal{T}_h} (f, v_T)_T + \sum_{F \in \mathcal{F}_h^\partial} (g, v_F)_F. \tag{20}$$

Then, the discrete problem reads: Find $\underline{\boldsymbol{u}}_h \in \underline{\boldsymbol{U}}_h^{k,0}$ such that,

$$a_h(\underline{\boldsymbol{u}}_h, \underline{\boldsymbol{v}}_h) = b_h(\underline{\boldsymbol{v}}_h) \quad \forall \underline{\mathbf{v}}_h \in \underline{\mathbf{U}}_h^{k,0}. \tag{21}$$

Introducing the global discrete gradient operator $G_h^k : \underline{\boldsymbol{U}}_h^k \to \bigtimes_{T \in \mathcal{T}_h} \nabla \mathbb{P}_d^{k+1}(T)$ such that, for each $\underline{\boldsymbol{v}}_h \in \underline{\boldsymbol{U}}_h^k$,

$$(G_h^k \underline{\boldsymbol{v}}_h)|_T := G_T^k \underline{\boldsymbol{v}}_T \quad \forall T \in \mathcal{T}_h, \tag{22}$$

we can reformulate the bilinear form a_h defined in (18) as

$$a_h(\underline{\boldsymbol{u}}_h, \underline{\boldsymbol{v}}_h) = (K G_h^k \underline{\boldsymbol{u}}_h, G_h^k \underline{\boldsymbol{v}}_h) + s_h(\underline{\boldsymbol{u}}_h, \underline{\boldsymbol{v}}_h). \tag{23}$$

To analyse the stability of the discrete problem, we introduce the local and global energy seminorms as follows:

$$\|\underline{\boldsymbol{v}}_h\|_{a,h}^2 := \sum_{T \in \mathcal{T}_h} \|\underline{\boldsymbol{v}}_T\|_{a,T}^2 \quad \text{where,} \quad \|\underline{\boldsymbol{v}}_T\|_{a,T}^2 := a_T(\underline{\boldsymbol{v}}_T . \underline{\boldsymbol{v}}_T), \tag{24}$$

Next result establishes an important relation between $\|\cdot\|_{a,T}$ and $\|\cdot\|_{K,T}$.

Lemma 3.1 *For any $\underline{\boldsymbol{v}}_T \in \underline{\boldsymbol{U}}_T^k$, there holds:*

$$\rho_T^{-1}\|\underline{\boldsymbol{v}}_T\|_{K,T}^2 \lesssim \|\underline{\boldsymbol{v}}_T\|_{a,T}^2 \lesssim \rho_T\|\underline{\boldsymbol{v}}_T\|_{K,T}^2. \tag{25}$$

Consequently, for all $\underline{\boldsymbol{v}}_h \in \underline{\boldsymbol{U}}_h^k$, $\|\underline{\boldsymbol{v}}_h\|_{K,h} \lesssim \|\underline{\boldsymbol{v}}_h\|_{a,h}$, and then, problem (21) is well-posed.

Proof. We refer to the proof of Lemma 3.1 in [9]. □

4 Error analysis

In this section we prove error estimates in the energy-norm and L^2-norm, under additional regularity assumption on exact solution.

Theorem 4.1 (Energy-error estimate) *Let $u \in U$ be the exact solution of (3) and let $\underline{\boldsymbol{u}}_h \in \underline{\boldsymbol{U}}_h^{k,0}$ be the solution of (21). We define the consistency error as $\mathcal{E}_h(\underline{\boldsymbol{v}}_h) := a_h(\underline{\mathrm{I}}_h^k u, \underline{\boldsymbol{v}}_h) - b_h(\underline{\boldsymbol{v}}_h)$. Then, recalling the definition of α (given in Lemma 2.3), and assuming that $u \in H^{k+2}(\mathcal{T}_h)$, there holds:*

$$\|\underline{\mathrm{I}}_h^k u - \underline{\boldsymbol{u}}_h\|_{a,h} \quad \leq \sup_{\underline{\boldsymbol{v}}_h \in \underline{\boldsymbol{U}}_h^{k,0},\, \|\underline{\boldsymbol{v}}_h\|_{a,h}=1} \mathcal{E}_h(\underline{\boldsymbol{v}}_h) \lesssim \left\{ \sum_{T\in\mathcal{T}_h} \overline{K}_T \rho_T^{2\alpha+1} h_T^{2(k+1)} \|u\|_{H^{k+2}(T)}^2 \right\}^{1/2}. \tag{26}$$

Moreover, applying Lemma 2.3, there holds

$$\|K^{1/2}(\nabla u - G_h^k \underline{\boldsymbol{u}}_h)\|_\Omega \lesssim \left\{ \sum_{T\in\mathcal{T}_h} \overline{K}_T \rho_T^{2\alpha+1} h_T^{2(k+1)} \|u\|_{H^{k+2}(T)}^2 \right\}^{1/2}. \tag{27}$$

Proof. We observe from (21) that $\mathcal{E}_h(\underline{\boldsymbol{v}}_h) = a_h(\underline{\mathrm{I}}_h^k u - \underline{\boldsymbol{u}}_h, \underline{\boldsymbol{v}}_h)$ for all $\underline{\boldsymbol{v}}_h \in \underline{\boldsymbol{U}}_h^{k,0}$. Then, the first inequality in (26) results from (24) and the fact that $\underline{\mathrm{I}}_h^k u - \underline{\boldsymbol{u}}_h \in \underline{\boldsymbol{U}}_h^{k,0}$.
Now, we derive a bound for the consistency error for a generic $\underline{\boldsymbol{v}}_h \in \underline{\boldsymbol{U}}_h^{k,0}$. Taking $w := p_T^k \underline{\mathrm{I}}_T^k u$ in the definition of $G_T^k \underline{\boldsymbol{v}}_T$ for all $T \in \mathcal{T}_h$, and using (10) and (22), we infer that

$$a_h(\underline{\mathrm{I}}_h^k u, \underline{\boldsymbol{v}}_h) = \sum_{T\in\mathcal{T}_h} \left\{ (\nabla v_T, K\nabla p_T^k \underline{\mathrm{I}}_T^k u)_T + \sum_{F\in\mathcal{F}_T} (v_F - v_T, K\nabla p_T^k \underline{\mathrm{I}}_T^k u \cdot \boldsymbol{n}_{TF})_F \right\} + s_h(\underline{\mathrm{I}}_h^k u, \underline{\boldsymbol{v}}_h). \tag{28}$$

Since $f = -\nabla\cdot(K\nabla u)$ in Ω (in distributional sense), an element-wise integration by parts in the first term of b_h yields

$$\sum_{T\in\mathcal{T}_h} (f, v_T)_T = \sum_{T\in\mathcal{T}_h} \left\{ (K\nabla u, \nabla v_T)_T - \sum_{F\in\mathcal{F}_T} (v_T, K\nabla u \cdot \boldsymbol{n}_{TF})_F \right\}. \tag{29}$$

In addition, from the fact that $g = K\nabla u \cdot \boldsymbol{n}$ on Γ (in distributional sense), we infer that the second term of b_h can write as

$$\sum_{F\in\mathcal{F}_h^\partial} (g, v_F)_F = \sum_{F\in\mathcal{F}_h^\partial} (v_F, K\nabla u \cdot \boldsymbol{n}_{TF})_F. \tag{30}$$

Then, from (29), (30) and noticing that v_F is single-valued on $\mathcal{F}_h$, and the fluxes $K\nabla u\cdot\boldsymbol{n}$ are continuous at interior faces, we infer that

$$b_h(\underline{\boldsymbol{v}}_h)=\sum_{T\in\mathcal{T}_h}\left\{(K\nabla u,\nabla v_T)_T+\sum_{F\in\mathcal{F}_T}(v_F-v_T,K\nabla u\cdot\boldsymbol{n}_{TF})_F\right\}. \tag{31}$$

Combining (28) with (31), we arrive at

$$\begin{aligned}\mathcal{E}_h(\underline{\boldsymbol{v}}_h)=&\sum_{T\in\mathcal{T}_h}\left\{\big(\nabla v_T,K\nabla(p_T^k\underline{\mathrm{I}}_T^k u-u)\big)_T+\sum_{F\in\mathcal{F}_T}\big(v_F-v_T,K\nabla(p_T^k\underline{\mathrm{I}}_T^k u-u)\cdot\boldsymbol{n}_{TF}\big)_F\right\}\\&+s_h(\underline{\mathrm{I}}_h^k u,\underline{\boldsymbol{v}}_h):=\mathfrak{T}_1+\mathfrak{T}_2.\end{aligned} \tag{32}$$

Aplying Cauchy-Schwarz inequality on each term of $\mathfrak{T}_1$, we obtain

$$\begin{aligned}|\mathfrak{T}_1|\le\sum_{T\in\mathcal{T}_h}&\left\{\rho_T^{-1/2}\|K^{1/2}\nabla v_T\|_T\,\rho_T^{1/2}\|K^{1/2}\nabla(p_T^k\underline{\mathrm{I}}_T^k u-u)\|_T\right.\\&\left.+\sum_{F\in\mathcal{F}_T}\rho_T^{-1/2}\left(\left\{\frac{k_F}{h_F}\right\}^{1/2}\|v_F-v_T\|_F\right)\rho_T^{1/2}\left(\left\{\frac{h_F}{k_F}\right\}^{1/2}\|\,K\nabla(p_T^k\underline{\mathrm{I}}_T^k u-u)\,\boldsymbol{n}_{TF}\|_F\right)\right\},\end{aligned} \tag{33}$$

Then, applying Cauchy-Schwarz inequality again, the fact that $\|K\nabla w\cdot\boldsymbol{n}_{TF}\|_F\le\|K^{1/2}\nabla w\|_F$, the mesh regularity property (4), and (15), we deduce

$$|\mathfrak{T}_1|\lesssim\left(\sum_{T\in\mathcal{T}_h}\rho_T\Big\{\|K^{1/2}\nabla(p_T^k\underline{\mathrm{I}}_T^k u-u)\|_T^2+h_T\|K^{1/2}\nabla(p_T^k\underline{\mathrm{I}}_T^k u-u)\|_{\partial T}^2\Big\}\right)^{1/2}\|\underline{\boldsymbol{v}}_h\|_{K,h}. \tag{34}$$

Next, by the approximation property (14) of $p_T^k\underline{\mathrm{I}}_T^k$, and the spectral norm of K, we infer that

$$\|K^{1/2}\nabla(p_T^k\underline{\mathrm{I}}_T^k u-u)\|_T^2+h_T\|K^{1/2}\nabla(p_T^k\underline{\mathrm{I}}_T^k u-u)\|_{\partial T}^2\lesssim\overline{\kappa}_T\rho_T^{2\alpha}h_T^{2(k+1)}\|u\|_{H^{k+2}(T)}^2. \tag{35}$$

Then, replacing (35) in (34), we derive

$$|\mathfrak{T}_1|\lesssim\left(\sum_{T\in\mathcal{T}_h}\overline{\kappa}_T\rho_T^{2\alpha+1}h_T^{2(k+1)}\|u\|_{H^{k+2}(T)}^2\right)^{1/2}\|\underline{\boldsymbol{v}}_h\|_{K,h}. \tag{36}$$

Next, we bound $\mathfrak{T}_2$. Applying triangle inequality and Cauchy-Schwarz inequality, we have

$$\big|s_h(\underline{\mathrm{I}}_h^k u,\underline{\boldsymbol{v}}_h)\big|\le s_h(\underline{\mathrm{I}}_h^k u,\underline{\mathrm{I}}_h^k u)^{1/2}\,s_h(\underline{\boldsymbol{v}}_h,\underline{\boldsymbol{v}}_h)^{1/2}. \tag{37}$$

Taking into account (17), the definition of $\underline{\mathrm{I}}_h^k u$, triangle inequality, discrete trace inequality and the L^2-stability of the projectors, we deduce

$$h_F^{-1/2}\|\pi_F^k(u-P_T^k\underline{\mathrm{I}}_h^k u)\|_F\lesssim h_F^{-1/2}\|u-p_T^k\underline{\mathrm{I}}_T^k u\|_F+h_F^{-1}\|u-p_T^k\underline{\mathrm{I}}_T^k u\|_T. \tag{38}$$

Now, since $k_F \leq \overline{K}_T$ for all $F \in \mathcal{F}_T$, together with the fact that card($\mathcal{F}_T$) is uniformly bounded, and the mesh regularity property (4), we infer from (38) that

$$\sum_{F\in\mathcal{F}_T} \frac{k_F}{h_F}\|\pi_F^k(u - P_T^k \underline{\mathrm{I}}_h^k u)\|_F^2 \lesssim \overline{K}_T\Big(h_T^{-1}\|u - p_T^k \underline{\mathrm{I}}_T^k u\|_{\partial T}^2 + h_T^{-2}\|u - p_T^k \underline{\mathrm{I}}_T^k u\|_T^2\Big). \tag{39}$$

Then, using (39), and the approximation property (14) of $p_T^k \underline{\mathrm{I}}_T^k$, we derive

$$s_T(\underline{\mathrm{I}}_T^k u, \underline{\mathrm{I}}_T^k u) \lesssim \overline{K}_T \rho_T^{2\alpha} h_T^{2(s-1)}\|u\|_{H^s(T)}^2 \quad \forall\, s \in \{2, \cdots, k+2\}. \tag{40}$$

Replacing (40) in (37) with $s = k+2$, we obtain

$$|\mathfrak{T}_2| \lesssim \left(\sum_{T\in\mathcal{T}_h} \overline{K}_T \rho_T^{2\alpha} h_T^{2(k+1)}\|u\|_{H^{k+2}(T)}^2\right)^{1/2} \|\underline{\boldsymbol{v}}_h\|_{a,h}. \tag{41}$$

Then, the second inequality in (26) results from (32), (36), (41), and the Lemma 3.1.
On the other hand, by triangle inequality, we obtain

$$\|K^{1/2}(\nabla u - G_h^k \underline{\boldsymbol{u}}_h)\|_\Omega \leq \|K^{1/2}(\nabla u - G_h^k \underline{\mathrm{I}}_h^k u)\|_\Omega + \|K^{1/2} G_h^k(\underline{\mathrm{I}}_h^k u - \underline{\boldsymbol{u}}_h))\|_\Omega \tag{42}$$

Finally, (27) follows from (42), (24), (26), and (35). □

Next, we provide an estimate of the L^2-error between u_h and $I_h^k u$ such that

$$u_h|_T := u_T \quad \text{and} \quad I_h^k u|_T := \pi_T^k u \qquad \forall\, T \in \mathcal{T}_h. \tag{43}$$

To this end, we need an additional elliptic regularity assumption in the following form: Given $w \in L_0^2(\Omega) := \{q \in L^2(\Omega) \,:\, (q,1)_\Omega = 0\}$, we let $z \in U$ be the unique function such that

$$(K\nabla z, \nabla v)_\Omega = (w, v)_\Omega \quad \forall v \in U, \tag{44}$$

which satisfies the a priori estimate:

$$\|z\|_{H^2(\Omega)} \lesssim \underline{K}^{-1}\|w\|_\Omega, \quad \underline{K} := \min_{T\in\mathcal{T}_h} \underline{K}_T. \tag{45}$$

Now, to establish the following result, we assume that K is a piecewise constant diffusivity tensor.

Theorem 4.2 (L^2-error estimate) *Under the assumptions of Theorem 4.1, elliptic regularity (45) and that $f \in H^k(\mathcal{T}_h)$, $g \in H^{k+1/2}(\mathcal{F}_h^\partial)$, there holds:*

$$\|I_h^k u - u_h\|_\Omega \lesssim \underline{K}^{-1}\Bigg((\overline{K})^{1/2}\rho h\Big\{\textstyle\sum_{T\in\mathcal{T}_h} \overline{K}_T \rho_T^2 h_T^{2(k+1)}\|u\|_{H^{k+2}(T)}^2\Big\}^{1/2} + h^{k+2}\Big\{\|f\|_{H^k(\mathcal{T}_h)} + \|g\|_{H^{k+1/2}(\mathcal{F}_h^\partial)}\Big\}\Bigg), \tag{46}$$

where, $\overline{K} := \max_{T\in\mathcal{T}_h} \overline{K}_T$, $\rho := \overline{K}/\underline{K}$, and $h := \max_{T\in\mathcal{T}_h} h_T$.

Proof. First, we set $e_h := I_h^k u - u_h \in L_0^2(\Omega)$ and $\underline{\boldsymbol{e}}_h := \underline{\mathrm{I}}_h^k u - \underline{\boldsymbol{u}}_h \in \underline{\boldsymbol{U}}_h^{k,0}$. Next, let $z \in U$ be the solution of (44) when considering $w := e_h$. Then, proceeding as in Theorem 4.1 for the auxiliary problem (44)-(45), we deduce

$$\|e_h\|_\Omega^2 = (e_h, w)_\Omega = \sum_{T\in\mathcal{T}_h} \left\{ (\nabla e_T, K\nabla z)_T - \sum_{F\in\mathcal{F}_T} (e_T, K\nabla z\cdot \boldsymbol{n}_{TF})_F \right\}. \tag{47}$$

Then, since $K\nabla z \in H(div,\Omega)$, and $K\nabla z\cdot\boldsymbol{n} = 0$ a.e. Γ, we can write (47) as

$$\|e_h\|_\Omega^2 = \sum_{T\in\mathcal{T}_h} \left\{ (\nabla e_T, K\nabla z)_T + \sum_{F\in\mathcal{F}_T} (e_F - e_T, K\nabla z\cdot \boldsymbol{n}_{TF})_F \right\}. \tag{48}$$

By taking, $\underline{\boldsymbol{v}}_h := \underline{\mathrm{I}}_h^k z \in \underline{\boldsymbol{U}}_h^{k,0}$ in (21), we infer that

$$a_h(\underline{\boldsymbol{e}}_h, \underline{\mathrm{I}}_h^k z) - a_h(\underline{\mathrm{I}}_h^k u, \underline{\mathrm{I}}_h^k z) + \sum_{T\in\mathcal{T}_h} (f, \pi_T^k z)_T + \sum_{F\in\mathcal{F}_h^\partial} (g, \pi_F^k z)_F = 0. \tag{49}$$

Besides, from the definition (23) and since $G_T^k \underline{\mathrm{I}}_T^k z = \nabla p_T^k \underline{\mathrm{I}}_T^k z$, we derive

$$a_h(\underline{\boldsymbol{e}}_h, \underline{\mathrm{I}}_h^k z) = \sum_{T\in\mathcal{T}_h} \Big\{ (\nabla e_T, K\nabla p_T^k \underline{\mathrm{I}}_T^k z)_T + \sum_{F\in\mathcal{F}_T} (e_F - e_T, K\nabla p_T^k \underline{\mathrm{I}}_T^k z\cdot \boldsymbol{n}_{TF})_F \Big\} + s_h(\underline{\boldsymbol{e}}_h, \underline{\mathrm{I}}_h^k z). \tag{50}$$

Combining (48) and (49) with (50), we arrive at

$$\begin{aligned}
\|e_h\|_\Omega^2 = &\left(a_h(\underline{\mathrm{I}}_h^k u, \underline{\mathrm{I}}_h^k z) - \sum_{T\in\mathcal{T}_h} (f, \pi_T^k z)_T - \sum_{F\in\mathcal{F}_h^\partial} (g, \pi_F^k z)_F \right) + \\
&\left(\sum_{T\in\mathcal{T}_h} \Big\{ \big(\nabla e_T, K\nabla (z - p_T^k \underline{\mathrm{I}}_T^k z)\big)_T + \sum_{F\in\mathcal{F}_T} \big(e_F - e_T, K\nabla (z - p_T^k \underline{\mathrm{I}}_T^k z)\cdot \boldsymbol{n}_{TF}\big)_F \Big\} - s_h(\underline{\boldsymbol{e}}_h, \underline{\mathrm{I}}_h^k z) \right) \\
&:= \mathfrak{T}_1 + \mathfrak{T}_2.
\end{aligned} \tag{51}$$

Now, testing the equation (3) with $v = z$, and reordering conveniently, we obtain

$$\begin{aligned}
\mathfrak{T}_1 = &\sum_{T\in\mathcal{T}_h} \Big\{ \big(K\nabla p_T^k \underline{\mathrm{I}}_T^k u, \nabla p_T^k \underline{\mathrm{I}}_T^k z\big)_T - (K\nabla u, \nabla z)_T \Big\} - \sum_{T\in\mathcal{T}_h} (f, \pi_T^k z - z)_T \\
&- \sum_{F\in\mathcal{F}_h^\partial} (g, \pi_F^k z - z)_F + s_h(\underline{\mathrm{I}}_h^k u, \underline{\mathrm{I}}_h^k z) := \mathfrak{T}_{1,1} + \mathfrak{T}_{1,2} + \mathfrak{T}_{1,3} + \mathfrak{T}_{1,4}.
\end{aligned} \tag{52}$$

To bound $\mathfrak{T}_{1,1}$, we write

$$\begin{aligned}
(K\nabla u, \nabla z)_T - \big(K\nabla p_T^k \underline{\mathrm{I}}_T^k u, \nabla p_T^k \underline{\mathrm{I}}_T^k z\big)_T = &\big(K\nabla (u - p_T^k \underline{\mathrm{I}}_T^k u), \nabla (z - p_T^k \underline{\mathrm{I}}_T^k z)\big)_T + \\
&\big(K\nabla (u - p_T^k \underline{\mathrm{I}}_T^k u), \nabla p_T^k \underline{\mathrm{I}}_T^k z)\big)_T + \big(K\nabla p_T^k \underline{\mathrm{I}}_T^k u, K\nabla (z - p_T^k \underline{\mathrm{I}}_T^k z)\big)_T .
\end{aligned} \tag{53}$$

The two last terms vanish by orthogonality property (12). Then, by approximation properties of $p_T^k \underline{\mathrm{I}}_T^k$ (14), Cauchy-Schwarz inequality, and (45) we deduce

$$|\mathfrak{T}_{1,1}| \lesssim \left(\sum_{T\in\mathcal{T}_h} \overline{K}_T \rho_T h_T^{2(k+1)} \|u\|^2_{H^{k+2}(T)} \right)^{1/2} \left(\sum_{T\in\mathcal{T}_h} \overline{K}_T \rho_T h_T^{2} \|z\|^2_{H^{2}(T)} \right)^{1/2}$$
$$\lesssim \underline{K}^{-1} (\overline{K})^{1/2} \rho^{1/2} h \left\{ \sum_{T\in\mathcal{T}_h} \overline{K}_T \rho_T h_T^{2(k+1)} \|u\|^2_{H^{k+2}(T)} \right\}^{1/2} \|e_h\|_\Omega \tag{54}$$

Turning to $\mathfrak{T}_{1,2}$, by the definition of $\pi_T^k z$, we can write $(f, \pi_T^k z - z)_T = (f - \pi_T^k f, \pi_T^k z - z)_T$. Then, applying approximation property (5) of π_T^k, Cauchy-Schwarz inequality and (45), we obtain

$$|\mathfrak{T}_{1,2}| \lesssim h^{k+2} \|f\|_{H^k(\Omega)} \|z\|_{H^2(\Omega)} \lesssim \underline{K}^{-1} h^{k+2} \|f\|_{H^k(\Omega)} \|e_h\|_{L^2(\Omega)}. \tag{55}$$

Proceeding similarly to bound $\mathfrak{T}_{1,3}$, first we notice that

$$\mathfrak{T}_{1,3} \;=\; - \sum_{F\in\mathcal{F}_h^\partial} (g - \Pi_F^k g, \pi_F^k z - z)_F \,.$$

For each $F \in \mathcal{F}_h^\partial$, we let $T_F \in \mathcal{T}_h$ be such that F is a face of ∂T_F. Then, applying Cauchy-Schwarz inequality, the fact that $\|\pi_F^k z - z\|_{L^2(F)} \le 2\|\pi_{T_F}^k z - z\|_{L^2(F)}$, and the approximation properties, we obtain

$$|\mathfrak{T}_{1,3}| \lesssim \sum_{F\in\mathcal{F}_h^\partial} h_{T_F}^{k+2} \|g\|_{H^{k+1/2}(F)} ||z||_{H^2(T_F)} \,.$$

After applying Minkowski inequality, we derive

$$|\mathfrak{T}_{1,3}| \lesssim h^{k+2} \left(\sum_{F\in\mathcal{F}_h^\partial} h_K^{k+2} \|g\|^2_{H^{k+1/2}(F)} \right)^{1/2} ||z||_{H^2(\Omega)} \,,$$

and then by (45)

$$|\mathfrak{T}_{1,3}| \lesssim \underline{K}^{-1} h^{k+2} \|g\|_{H^{k+1/2}(\mathcal{F}_h^\partial)} ||e_h||_{L^2(\Omega)} \,. \tag{56}$$

To estimate $\mathfrak{T}_{1,4}$, we apply triangle inequality, Cauchy-Schwarz inequality, the bound (40), and (45), obtaining

$$|\mathfrak{T}_{1,4}| \le s_h(\underline{\mathrm{I}}_h^k u, \underline{\mathrm{I}}_h^k u)^{1/2} \, s_h(\underline{\mathrm{I}}_h^k z, \underline{\mathrm{I}}_h^k z)^{1/2}$$
$$\lesssim \underline{K}^{-1} (\overline{K})^{1/2} \rho^{1/2} h \left\{ \sum_{T\in\mathcal{T}_h} \overline{K}_T \rho_T h_T^{2(k+1)} \|u\|^2_{H^{k+2}(T)} \right\}^{1/2} \|e_h\|_{L^2(\Omega)}. \tag{57}$$

Then, we infer from (54)-(57) that

$$|\mathfrak{T}_1| \;\lesssim\; \underline{K}^{-1} \Bigg((\overline{K})^{1/2} \rho^{1/2} h \left\{ \sum_{T\in\mathcal{T}_h} \overline{K}_T \rho_T h_T^{2(k+1)} \|u\|^2_{H^{k+2}(T)} \right\}^{1/2}$$
$$+ h^{k+2} \left\{ \|f\|_{H^k(\mathcal{T}_h)} + \|g\|_{H^{k+1/2}(\mathcal{F}_h^\partial)} \right\} \Bigg) \; \|e_h\|_{L^2(\Omega)}.$$

Now, we denote by $\mathfrak{T}_{2,1}$, $\mathfrak{T}_{2,2}$ the two terms of $\mathfrak{T}_2$. Proceeding as in the proof of Theorem 4.1, we bound $\mathfrak{T}_{2,1}$ by considering (36), the Lemma 3.1, (26) and the elliptic regularity property (45)

$$
\begin{aligned}
|\mathfrak{T}_{2,1}| &\lesssim \|\underline{\boldsymbol{e}}_h\|_{K,h}\left\{\sum_{T\in\mathcal{T}_h}\overline{K}_T\rho_T^2 h_T^{2(k+1)}\|z\|^2_{H^2(T)}\right\}^{1/2}\\
&\lesssim (\overline{K})^{1/2}\rho h\left\{\sum_{T\in\mathcal{T}_h}\overline{K}_T\rho_T^2 h_T^{2(k+1)}\|u\|^2_{H^{k+2}(T)}\right\}^{1/2}\|z\|_{H^2(\Omega)}\\
&\lesssim \underline{K}^{-1}(\overline{K})^{1/2}\rho h\left\{\sum_{T\in\mathcal{T}_h}\overline{K}_T\rho_T^2 h_T^{2(k+1)}\|u\|^2_{H^{k+2}(T)}\right\}^{1/2}\|e_h\|_{\Omega} \qquad (58)
\end{aligned}
$$

Turning to $\mathfrak{T}_{2,2}$, we take into account (41), (26) and (45), to obtain

$$
\begin{aligned}
|\mathfrak{T}_{2,2}| &\leq s_h(\underline{\boldsymbol{e}}_h,\underline{\boldsymbol{e}}_h)^{1/2}\; s_h(\underline{\mathrm{I}}_h^k z,\underline{\mathrm{I}}_h^k z)^{1/2}\\
&\lesssim (\overline{K})^{1/2}\rho^{1/2}h\left\{\sum_{T\in\mathcal{T}_h}\overline{K}_T\rho_T^2 h_T^{2(k+1)}\|u\|^2_{H^{k+2}(T)}\right\}^{1/2}\|z\|_{H^2(\Omega)}\\
&\lesssim \underline{K}^{-1}(\overline{K})^{1/2}\rho^{1/2}h\left\{\sum_{T\in\mathcal{T}_h}\overline{K}_T\rho_T^2 h_T^{2(k+1)}\|u\|^2_{H^{k+2}(T)}\right\}^{1/2}\|e_h\|_{\Omega}. \qquad (59)
\end{aligned}
$$

Finally, we conclude the proof from (58)-(59). □

5 Implementation

For computational implementation purposes, finding a basis for $\underline{\boldsymbol{U}}_h^{k,0}$ could be a hard task, due to the zero mean value condition that must satisfy all its elements. One way to circumvent this difficulty, is to impose this restriction with the help of a Lagrange multiplier. This lets us to introduce the following discrete scheme, which reads as: Find $(\underline{\boldsymbol{u}}_h,\lambda)\in\underline{\boldsymbol{U}}_h^k\times\mathbb{R}$ such that

$$
a_h(\underline{\boldsymbol{u}}_h,\underline{\boldsymbol{v}}_h)+\lambda(v_h,1)_\Omega+\mu(u_h,1)_\Omega = b_h(\underline{\boldsymbol{v}}_h)\quad \forall\,(\underline{\boldsymbol{v}}_h,\mu)\in\underline{\boldsymbol{U}}_h^k\times\mathbb{R}. \qquad (60)
$$

Theorem 5.1 *The problems (21) and (60) are equivalent, in the sense:*

1. *If $(\underline{\boldsymbol{u}}_h,\lambda)$ is a solution of (60), then $\lambda=0$ and $\underline{\boldsymbol{u}}_h\in\underline{\boldsymbol{U}}_h^{k,0}$ solution of (21).*
2. *If $\underline{\boldsymbol{u}}_h\in\underline{\boldsymbol{U}}_h^{k,0}$ is a solution of (21), then $(\underline{\boldsymbol{u}}_h,0)\in\underline{\boldsymbol{U}}_h^k\times\mathbb{R}$ is a solution of (60).*

Proof. It is immediate from the compatibility condition (2). □

To deduce associated linear system to (60), we rewrite the term b_h as

$$
b_h(\underline{\boldsymbol{v}}_h) := \sum_{T\in\mathcal{T}_h} b_T(\underline{\boldsymbol{v}}_T)\quad,\quad b_T(\underline{\boldsymbol{v}}_T) := (f,v_T)_T + \sum_{F\in\mathcal{F}_T\cap\mathcal{F}_h^\partial}(g,v_F)_F. \qquad (61)
$$

For integers $l \geq 0$ and $n \geq 0$, we denote by $N_n^l := \begin{pmatrix} l+n \\ l \end{pmatrix}$ the dimension of the space composed of n-variate polynomials of degree at most l.

For any $\underline{\boldsymbol{v}}_h$ in the global discrete space $\underline{\boldsymbol{U}}_h^k$, we collect its components with respect to the polynomial bases attached to the mesh cells and faces in a global component vector denoted by $V_{\mathcal{TF}} \in \mathbb{R}^{N_{\mathcal{T}}^k}$ with

$$N_{\mathcal{T}}^k := \dim(\underline{\boldsymbol{U}}_h^k) = \mathrm{card}(\mathcal{T}_h) \times N_d^k + \mathrm{card}(\mathcal{F}_h) \times N_{d-1}^k, \tag{62}$$

where N_d^k and N_{d-1}^k denote the dimension of the local cell and face bases, respectively, while d represents the space dimension. We can decompose the global vector of coefficients as

$$V_{\mathcal{TF}} = \left[\begin{array}{c} V_{\mathcal{T}} \\ \hdashline V_{\mathcal{F}} \end{array}\right], \tag{63}$$

where the vectors $V_{\mathcal{T}}$ and $V_{\mathcal{F}}$ collect the coefficients associated to element-based and face-based DOFS, respectively.

Also, we can collect, for every $\underline{\boldsymbol{v}}_T \in \underline{\boldsymbol{U}}_T^k$, its components associated to T and ∂T, in a local component vector denoted by $V_{T\mathcal{F}_T} \in \mathbb{R}^{N_T^k}$, and in the similar way, we split the local vector of coefficients associated to the element T as

$$V_{T\mathcal{F}_T} = \left[\begin{array}{c} V_T \\ \hdashline V_{\mathcal{F}_T} \end{array}\right], \tag{64}$$

with V_T and $V_{\mathcal{F}_T}$ collecting the coefficients associated to the bases of the element and faces linked to T, respectively.

Expressing the functions in the discrete formulation (60) as a linear combination of its respective basis functions, we obtain the following problem: Find $(U_{\mathcal{TF}}, \lambda) \in \mathbb{R}^{N_{\mathcal{T}}^k} \times \mathbb{R}$ such that

$$\sum_{T\in\mathcal{T}_h} V_{T\mathcal{F}_T}^T A(T) U_{T\mathcal{F}_T} + \lambda \sum_{T\in\mathcal{T}_h} V_T^T M_T + \mu \sum_{T\in\mathcal{T}_h} M_T^T U_T = \sum_{T\in\mathcal{T}_h} V_{T\mathcal{F}_T}^T B(T), \tag{65}$$

for all $(V_{\mathcal{TF}}, \mu) \in \mathbb{R}^{N_{\mathcal{T}}^k} \times \mathbb{R}$. Here, the local matrix $A(T)$ represents the local bilinear form a_T, the local vector $B(T)$ represents the linear functional b_T, and the vector $M_T \in \mathbb{R}^{N_d^k}$ collects the average of the local base functions on T:

$$A(T) = \left[\begin{array}{c:c} A_{TT} & A_{T\mathcal{F}_T} \\ \hdashline A_{T\mathcal{F}_T}^T & A_{\mathcal{F}_T\mathcal{F}_T} \end{array}\right], \qquad B(T) = \left[\begin{array}{c} B_T \\ \hdashline B_{\mathcal{F}_T} \end{array}\right], \tag{66}$$

Arranging the equation (65) in a matrix form, in order to eliminate the element-based DOFS (by static condensation), we obtain the following linear global system corresponding to the discrete problem (60):

$$\left[\begin{array}{c:c:c} A_{\mathcal{TT}} & A_{\mathcal{TF}} & M_{\mathcal{T}} \\ \hdashline A_{\mathcal{TF}}^T & A_{\mathcal{FF}} & 0_{\mathcal{F}} \\ \hdashline M_{\mathcal{T}}^T & 0_{\mathcal{F}}^T & 0 \end{array}\right] \left[\begin{array}{c} U_{\mathcal{T}} \\ \hdashline U_{\mathcal{F}} \\ \hdashline \lambda \end{array}\right] = \left[\begin{array}{c} B_{\mathcal{T}} \\ \hdashline B_{\mathcal{F}} \\ \hdashline 0 \end{array}\right], \tag{67}$$

where the vector $M_{\mathcal{T}} \in \mathbb{R}^{N_{\mathcal{T}}^k}$ denote the vector collecting the average of the functions of the element-based DOFs, and $0_{\mathcal{F}}$ is the zero vector in $\mathbb{R}^{\mathrm{card}(\mathcal{F}_h)\times N_{d-1}^k}$, and the number of unknowns is

$$\mathrm{card}(\mathcal{T}_h) \times N_d^k + \mathrm{card}(\mathcal{F}_h) \times N_{d-1}^k + 1. \tag{68}$$

Instead of assembling the full system (67), we can effectively compute the Schur complement of $A_{\mathcal{T}\mathcal{T}}$, following the system

$$A_{\mathcal{T}\mathcal{T}} U_{\mathcal{T}} + \widehat{A}_{\mathcal{T}\mathcal{F}} \widehat{U}_{\mathcal{F}} = B_{\mathcal{T}}, \tag{69}$$

$$\widehat{A}_{\mathcal{T}\mathcal{F}}^T U_{\mathcal{T}} + \widehat{A}_{\mathcal{F}\mathcal{F}} \widehat{U}_{\mathcal{F}} = \widehat{B}_{\mathcal{F}}, \tag{70}$$

where

$$\widehat{A}_{\mathcal{F}\mathcal{F}} = \left[\begin{array}{c:c} A_{\mathcal{F}\mathcal{F}} & 0_{\mathcal{F}} \\ \hdashline 0_{\mathcal{F}}^T & 0 \end{array}\right], \ \widehat{A}_{\mathcal{T}\mathcal{F}} = \left[\begin{array}{c:c} A_{\mathcal{T}\mathcal{F}} & M_{\mathcal{T}} \end{array}\right], \ \widehat{U}_{\mathcal{F}} = \left[\begin{array}{c:c} U_{\mathcal{F}} & \lambda \end{array}\right]^T, \text{ and } \widehat{B}_{\mathcal{F}} = \left[\begin{array}{c:c} B_{\mathcal{F}} & 0 \end{array}\right]^T.$$

From (69), we obtain

$$U_{\mathcal{T}} = A_{\mathcal{T}\mathcal{T}}^{-1} \left[B_{\mathcal{T}} - \widehat{A}_{\mathcal{T}\mathcal{F}} \widehat{U}_{\mathcal{F}} \right]. \tag{71}$$

Then, replacing (71) in (70), we derive

$$\left[\widehat{A}_{\mathcal{F}\mathcal{F}} - \widehat{A}_{\mathcal{T}\mathcal{F}}^T A_{\mathcal{T}\mathcal{T}}^{-1} \widehat{A}_{\mathcal{T}\mathcal{F}} \right] \widehat{U}_{\mathcal{F}} = \left[\widehat{B}_{\mathcal{F}} - \widehat{A}_{\mathcal{T}\mathcal{F}}^T A_{\mathcal{T}\mathcal{T}}^{-1} B_{\mathcal{T}} \right]. \tag{72}$$

After simplifying the system (72), we obtain the following reduced system, where the element-based DOFs collected in the vector $U_{\mathcal{T}}$ no longer appears:

$$\left[\begin{array}{c:c} A_{\mathcal{F}\mathcal{F}} - A_{\mathcal{T}\mathcal{F}}^T A_{\mathcal{T}\mathcal{T}}^{-1} A_{\mathcal{T}\mathcal{F}} & -A_{\mathcal{T}\mathcal{F}}^T A_{\mathcal{T}\mathcal{T}}^{-1} M_{\mathcal{T}} \\ \hdashline -M_{\mathcal{T}}^T A_{\mathcal{T}\mathcal{T}}^{-1} A_{\mathcal{T}\mathcal{F}} & -M_{\mathcal{T}}^T A_{\mathcal{T}\mathcal{T}}^{-1} M_{\mathcal{T}} \end{array}\right] \left[\begin{array}{c} U_{\mathcal{F}} \\ \hdashline \lambda \end{array}\right] = \left[\begin{array}{c} B_{\mathcal{F}} - A_{\mathcal{T}\mathcal{F}}^T A_{\mathcal{T}\mathcal{T}}^{-1} B_{\mathcal{T}} \\ \hdashline -M_{\mathcal{T}}^T A_{\mathcal{T}\mathcal{T}}^{-1} B_{\mathcal{T}} \end{array}\right]. \tag{73}$$

The advantage of implementing the reduced system (73) over the global system (67) is that the number of unknowns in (73) is reduced to

$$\mathrm{card}(\mathcal{F}_h) \times N_{d-1}^k + 1. \tag{74}$$

Denoting by $\underset{T\in\mathcal{T}_h}{\longleftarrow}$ the usual assembling procedure based on a global DOF map, we can assemble all matrix products appearing in (73) directly from their local counterparts, as

$$B_{\mathcal{F}} - A_{\mathcal{T}\mathcal{F}}^T A_{\mathcal{T}\mathcal{T}}^{-1} B_{\mathcal{T}} \underset{T\in\mathcal{T}_h}{\longleftarrow} B_{\mathcal{F}_T} - A_{T\mathcal{F}_T}^T A_{TT}^{-1} B_T \quad , \quad A_{\mathcal{T}\mathcal{F}}^T A_{\mathcal{T}\mathcal{T}}^{-1} M_{\mathcal{T}} \underset{T\in\mathcal{T}_h}{\longleftarrow} A_{T\mathcal{F}_T}^T A_{TT}^{-1} M_T,$$
$$A_{\mathcal{F}\mathcal{F}} - A_{\mathcal{T}\mathcal{F}}^T A_{\mathcal{T}\mathcal{T}}^{-1} A_{\mathcal{T}\mathcal{F}} \underset{T\in\mathcal{T}_h}{\longleftarrow} A_{\mathcal{F}_T\mathcal{F}_T} - A_{T\mathcal{F}_T}^T A_{TT}^{-1} A_{T\mathcal{F}_T},$$

$$M_{\mathcal{T}}^T A_{\mathcal{T}\mathcal{T}}^{-1} M_{\mathcal{T}} = \sum_{T\in\mathcal{T}_h} M_T^T A_{TT}^{-1} M_T, \text{and} \quad M_{\mathcal{T}}^T A_{\mathcal{T}\mathcal{T}}^{-1} B_{\mathcal{T}} = \sum_{T\in\mathcal{T}_h} M_T^T A_{TT}^{-1} B_T.$$

Besides, the global vector $U_{\mathcal{T}}$ can be recovered from (69), letting $\lambda = 0$ in $\widehat{U}_{\mathcal{F}}$, so that

$$U_{\mathcal{T}} = A_{\mathcal{T}\mathcal{T}}^{-1} \Big(B_{\mathcal{T}} - A_{\mathcal{T}\mathcal{F}} U_{\mathcal{F}} \Big), \tag{75}$$

Finally, for all $T \in \mathcal{T}_h$, the local vector U_T of element-based DOFs can be recovered from (75) following element-by-element post-processing:

$$U_T = A_{TT}^{-1} \Big(B_T - A_{T\mathcal{F}_T} U_{\mathcal{F}_T} \Big). \tag{76}$$

6 Numerical results

In this section we present a comprehensive set of numerical tests to assess the properties of our method. We use different meshes for the numerical tests, which were originally prosed for the FVCA5 benchmark [19].

We based our code on the one developed by Di Pietro ([8],[11]), where, the implementation of local gradient reconstruction (9), L^2-orthogonal projectors π_T^k and π_F^k, are based on the linear algebra facilities (robust Cholesky factorization) provided by the Eigen3 library [18]. The reduced system on the skeleton (73) is solved using SuperLU [5] through the PETSc 3.4 interface [2].

For each of the examples presented here, we consider four meshes family, which are depicted in Figure 1. In addition, we compute the experimental order of convergence (r) as

$$r = \log(e_{\mathcal{T}_1}/e_{\mathcal{T}_2})/\log(h_{\mathcal{T}_1}/h_{\mathcal{T}_2})\,,$$

where $e_{\mathcal{T}_1}$ and $e_{\mathcal{T}_2}$ are the errors associated to the corresponding variable considering two consecutive meshsizes $h_{\mathcal{T}_1}$ and $h_{\mathcal{T}_2}$, respectively.

6.1 Example 1: Constant diffusivity

First, we consider a Neumann problem defined in $\Omega := (0,1)^2$, whose data are such that its exact solution is given by the smooth function

$$u(x,y) = \sin(\pi x)\sin(\pi y) - \frac{4}{\pi^2}\,, \tag{77}$$

with diffusivity tensor $K := \boldsymbol{I}$. Tables 1 and 2 show the behavior of potential an flux errors, for each one of the described triangulations. In all cases, it is noticed that the scheme converges, and it does at the expected optimal rates of convergence: $k+2$ for the potential, and $k+1$ for the flux, when the solution is approximated by piecewise polynomials of degree at most k. This is in agreement with Theorems 4.1 and 4.2, and it can be observed in Figure 2.

6.2 Example 2: Polynomial diffusivity

The aim here is to check the robustness of the method, when we solve on the unit square domain $\Omega = (0,1)^2$ the non-homogeneous Neumann problem with

$$u(x,y) = \sin(\pi x)\sin(\pi y) - \frac{4}{\pi^2}, \tag{78}$$

and diffusion tensor (from [20]):

$$K(x,y) = \begin{pmatrix} (y-\bar{y})^2 + \epsilon(x-\bar{x})^2 & -(1-\epsilon)(x-\bar{x})(y-\bar{y}) \\ -(1-\epsilon)(x-\bar{x})(y-\bar{y}) & (x-\bar{x}) + \epsilon(y-\bar{y})^2 \end{pmatrix}, \tag{79}$$

where $(\bar{x},\bar{y}) = -(0.1,0.1)$. This defines an anisotropic problem, where the principal axes of the diffusion tensor vary at each point of the domain. For the case $\epsilon = 10^{-1}$, we obtain an anisotropic ratio $\rho = 10$. Figure 3 exhibits the well behavior of the Potential (first column) and

Flux (second column) L^2-errors with respect to the mesh size h, and for each one of the four meshes family. Their corresponding histories of convergence are given in Tables 3 and 4, and they are in agreement with Theorems 4.1 and 4.2, despite the fact that it is not covered (at all) by the theory since K is not piecewise constant (as required for proving Theorem 4.2). This gives some numerical evidence that our results could be improved for a general kind of diffusivity tensor.

6.3 Example 3: Neumann problem with numerical singularity

Here, we consider the Neumann problem on the unit square domain $\Omega = (0,1)^2$, where its data are such that the exact solution is given by the potential function:

$$u(x,y) = \frac{xy}{(x+0.05)^2 + y^2} - \overline{u}\,, \tag{80}$$

with homogeneous anisotropic diffusion tensor:

$$K(x,y) = \begin{pmatrix} 1.5 & 0.5 \\ 0.5 & 1.5 \end{pmatrix}. \tag{81}$$

We remark that $\overline{u}$ represents the mean value of u in Ω, and notice that u has a singularity at $(-0.05, 0)$, which is close to $\partial\Omega$. The history of errors for potential and flux are shown in Tables 5 and 6, for $k \in \{0,1,2,3\}$, and for each of the four considered triangulations. For the first three triangulations, they exhibit that the HHO method converges with the corresponding optimal rate of convergence $k+2$ and $k+1$ for the potential and flux error, respectively. This is also observed in Figure 4. For the latter triangulation, we observe that the order of convergence behaves as $k+1$ and k, respectively. This phenomena could be explained since the sequence of uniformed hexagonal meshes does not refine enough in the neighborhood of $(-0.05, 0)$, and then it is not capable of capturing the induced numerical singularity. This should be improve by performing certain a posteriori error adaptivity procedure, which would be the subject of future work.

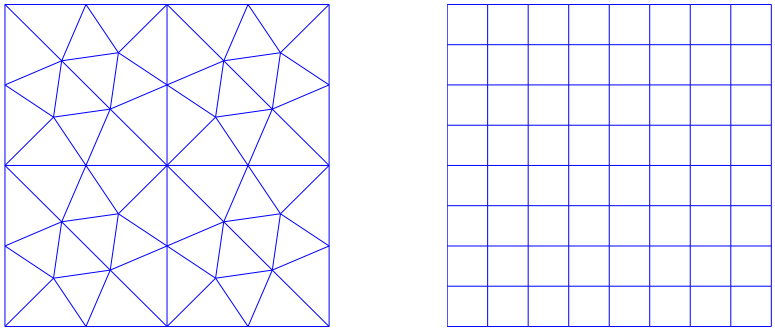

(a) Triangular (b) Cartesian

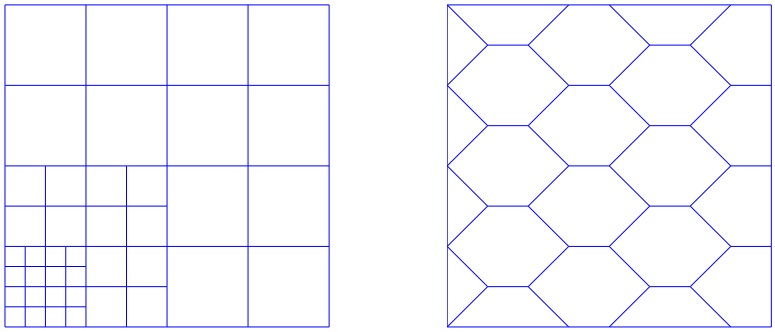

(c) Refined (d) Hexagonal

Figure 1: Triangular, Cartesian, Refined and Hexagonal initial meshes that define the triangulations considered for the numerical examples.

Conclusions

In this work we have developed an a priori error analysis for a pure Neumann problem, when applying HHO method. We have proved the convergence of the method, with the optimal rates of convergence when the exact solution is smooth enough: order $k+1$ for the flux error, and $k+2$ for potential error. This technique can deal with hanging nodes, as in the Refined mesh (Figure 1c), and also with general element (Figure 1a, 1b and 1d). Although we do not show 3D examples, it is possible to work with meshes in 3D. For that purpose, we refer to the library, named DiSk++, which is available as open-source, under MPL License, at the address `https://github.com/datafl4sh/diskpp`. Numerical results presented here, are in agreement with our theoretical results, although is possible to extent the Theorem 4.2 to general tensor as in the Example 2. These allow us to extend this technique to solve a linear transmission problem with Neumann condition, in a bounded region of the plane. This will be report in a separate work, which at the present, is under development.

Acknowledgements

R. Bustinza has been partially supported by CONICYT-Chile through project AFB170001 of the PIA Program: Concurso Apoyo a Centros Científicos y Tecnológicos de Excelencia con Financiamiento Basal, by project VRID-Enlace No. 218.013.044-1.0, Universidad de Concepción, and by Centro de Investigación en Ingeniería Matemática (CI^2MA), Universidad de Concepción (Chile). J. Munguia wishes to express their thanks for the financial support of CONCYTEC-Perú through FONDECYT project "Programas de Doctorado en Universidades Peruanas" CG-176-2015, to Instituto de Matemática y Ciencias Afines (IMCA) and to Universidad Nacional de Ingeniería (Lima-Perú). On the other hand, J. Munguia would like to thank Centro de Investigación en Ingeniería Matemática (CI^2MA), Universidad de Concepción (Chile), for the kind hospitality and facilities that was offered to him during his visits to this center. In addition, R. Bustinza wishes to express his gratitude to Instituto de Matemática y Ciencias Afines (IMCA), for making each one of his stays at this institute feels like home.

References

[1] B. Ayuso de Dios, K. Lipnikov, and G. Manzini: *The nonconforming virtual element method*, ESAIM: Math. Model. Numer. Anal. (M2AN), 50(3):879904, 2016.

[2] S. Balay, J. Brown, K. Buschelman, W. D. Gropp, D. Kaushik, M. G. Knepley, L. Curfman McInnes, B. F. Smith, and H. Zhang. PETSc Web page. `http://www.mcs.anl.gov/petsc`, 2011.

[3] M. Cicuttin, D. A. Di Pietro, and A. Ern: *Implementation of Discontinuous Skeletal methods on arbitrary-dimensional, polytopal meshes using generic programming*, Journal of Computational and Applied Mathematics, 344, 852-874, 2018.

[4] B. Cockburn, D. A. Di Pietro, and A. Ern: *Bridging the Hybrid High-Order and Hybridizable Discontinuous Galerkin methods*, ESAIM: Math. Model Numer. Anal. (M2AN), 50(3):635-650, 2015. Published online. DOI: 10.1051/m2an/2015051.

[5] J. W. Demmel, S. C. Eisenstat, J. R. Gilbert, X. S. Li, and J. W. H. Liu. A supernodal approach to sparse partial pivoting. SIAM J. Matrix Analysis and Applications, 20 (3):720-755, 1999.

[6] D. A. Di Pietro, and J. Droniou: *A Hybrid High-Order method for Leray–Lions elliptic equations on general meshes*, Mathematics of Computation, 86 (307), 2159-2191, 2017.

[7] D. A. Di Pietro, and A. Ern: *Mathematical aspects of discontinuous Galerkin methods*, volume 69 of Mathématiques & Applications. Springer-Verlag, Berlin, 2012.

[8] D. A. Di Pietro, A. Ern, and S. Lemaire: *An arbitrary-order and compact-stencil discretization of diffusion on general meshes based on local reconstruction operators*, Computer Methods in Applied Mathematics, 14 (4), 461-472, 2014.

[9] D. A. Di Pietro, and A. Ern: *Hybrid High-Order methods for variable-diffusion problems on general meshes*, Comptes Rendus Mathématique. Académie des Sciences. Paris, 353 (1), 31-34, 2015.

[10] D. A. Di Pietro and A. Ern: *Arbitrary-order mixed methods for heterogeneous anisotropic diffusion on general meshes*, IMA J. Numer. Anal., 2016. Published online. DOI 10.1093/imanum/drw003.

[11] D. A. Di Pietro, and A. Ern: *A hybrid high-order locking-free method for linear elasticity on general meshes*, Comput. Meth. Appl. Mech. Engrg., 283, 1-21, 2015.

[12] D. A. Di Pietro, A. Ern, and S. Lemaire: *A review of Hybrid High-Order methods: formulations, computational aspects, comparison with other methods*, In G. R. Barrenechea, F. Brezzi, A. Cangiani, and E. H. Georgoulis, editors, Building Bridges: Connections and Challenges in Modern Approaches to Numerical Partial Differential Equations, volume 114 of Lecture Notes in Computational Science and Engineering, pages 205-236, Switzerland, 2016. Springer.

[13] J. Droniou and R. Eymard: *A mixed finite volume scheme for anisotropic diffusion problems on any grid*, Numer. Math., 105, 35-71, 2006.

[14] J. Droniou, R. Eymard, T. Gallouët, C. Guichard, and R. Herbin: *The gradient discretisation method*, Mathématiques & Applications, vol. 82. Springer, 2018. DOI: 10.1007/978-3-319-79042-8.

[15] R. Eymard, T. Gallouët, and R. Herbin: *Discretization of heterogeneous and anisotropic diffusion problems on general nonconforming meshes. SUSHI: a scheme using stabilization and hybrid interfaces*. IMA J. Numer. Anal., 30 (4), 1009-1043, 2010.

[16] G. N. Gatica. Introducción al Análisis Funcional. Editorial Reverté, S. A., 2014.

[17] G.N. Gatica, and F.J. Sayas: A note on the local approximation properties of piecewise polynomials with applications to LDG methods. Complex Variables and Elliptic Equations, vol. 51, (2), pp. 109-117, (2006).

[18] G. Guennebaud and B. Jacob. Eigen v3. `http://eigen.tuxfamily.org`, 2010.

[19] R. Herbin, and F. Hubert: *Benchmark on discretization schemes for anisotropic diffusion problems on general grids*, In R. Eymard and J.-M. Hrard, editors, Finite Volumes for Complex Applications V, pages 659692. John Wiley & Sons, 2008.

[20] C. Le Potier: *A finite volume method for the approximation of highly anisotropic diffusion operators on unstructured meshes*, in: Finite volumes for complex applications IV, ISTE, London, 2005, pp. 401-412.

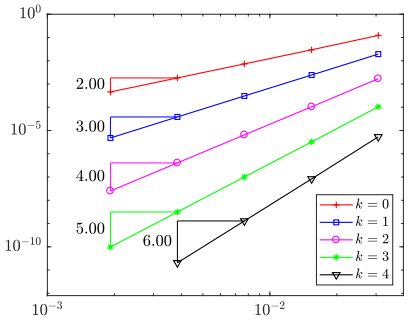

(a) Potential error, Triangular meshes

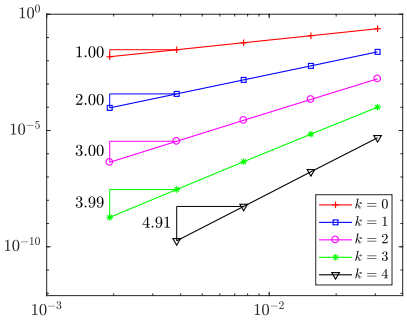

(b) Flux error, Triangular meshes

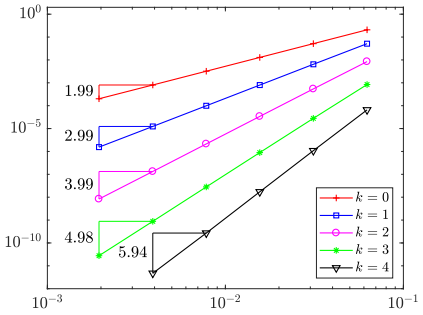

(c) Potential error, Cartesian meshes

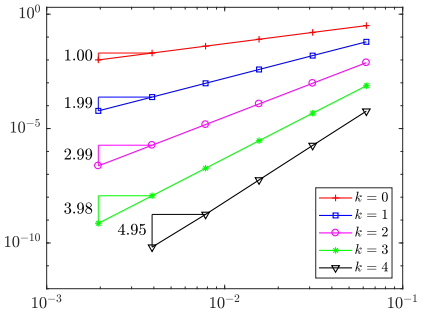

(d) Flux error, Cartesian meshes

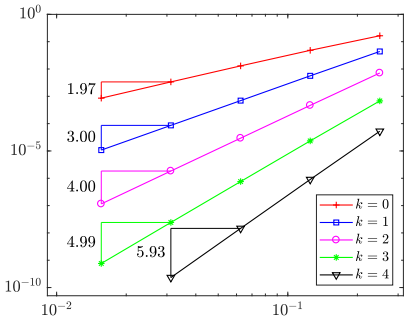

(e) Potential error, Refined meshes

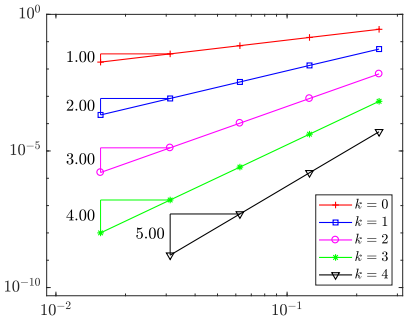

(f) Flux error, Refined meshes

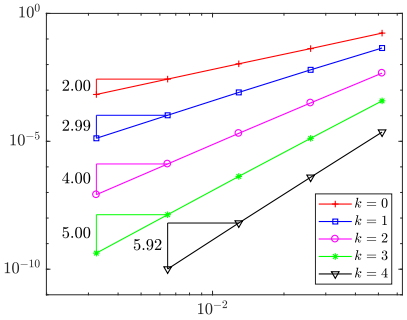

(g) Potential error, Hexagonal meshes

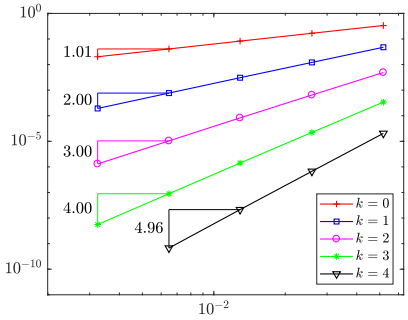

(h) Flux error, Hexagonal meshes

Figure 2: Rates of convergence of Potential and Flux errors, considering each one of the four triangulations (Example 1).

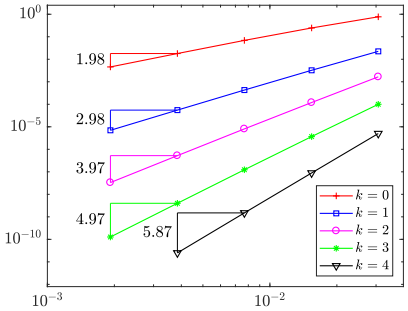

(a) Potential error, Triangular meshes

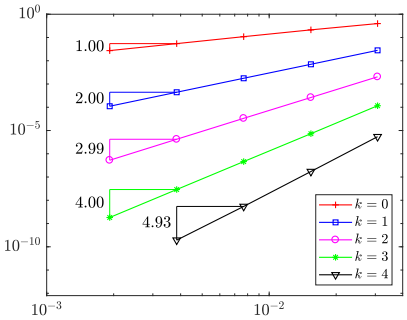

(b) Flux error, Triangular meshes

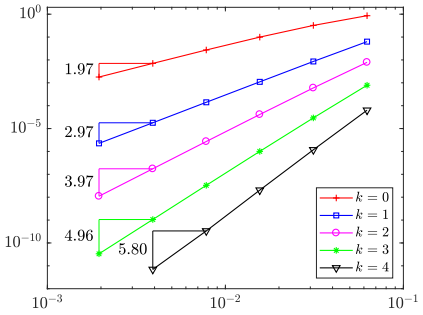

(c) Potential error, Cartesian meshes

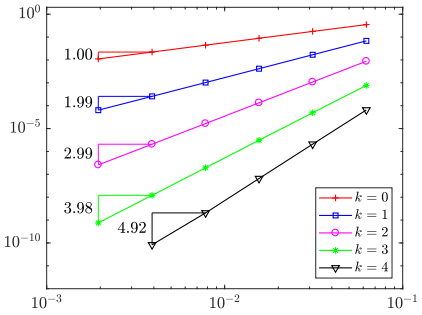

(d) Flux error, Cartesian meshes

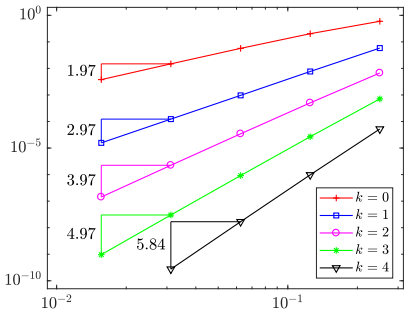

(e) Potential error, Refined meshes

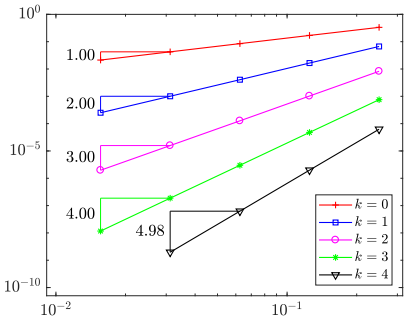

(f) Flux error, Refined meshes

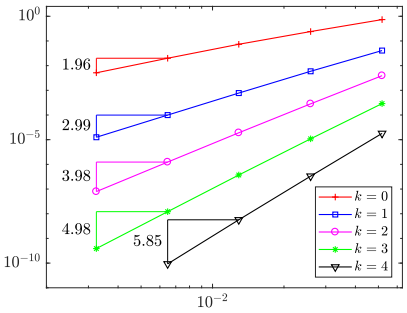

(g) Potential error, Hexagonal meshes

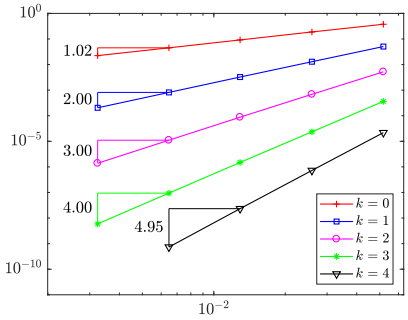

(h) Flux error, Hexagonal meshes

Figure 3: Rates of convergence of potential and flux errors, considering each one of the four triangulations (Example 2).

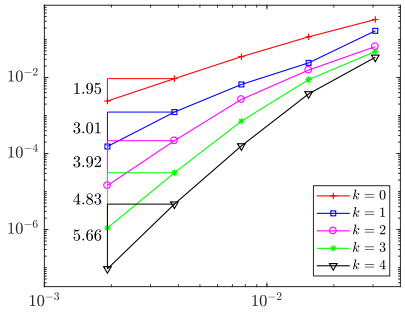

(a) Potential error, Triangular meshes

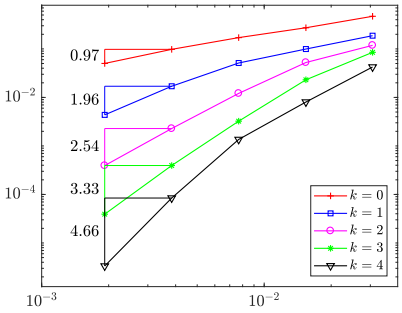

(b) Flux error, Triangular meshes

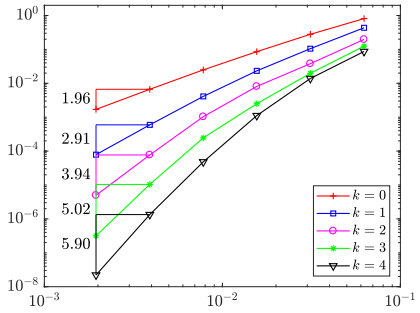

(c) Potential error, Cartesian meshes

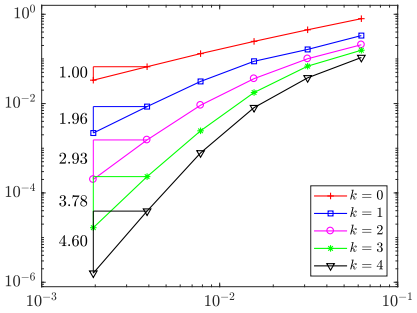

(d) Flux error, Cartesian meshes

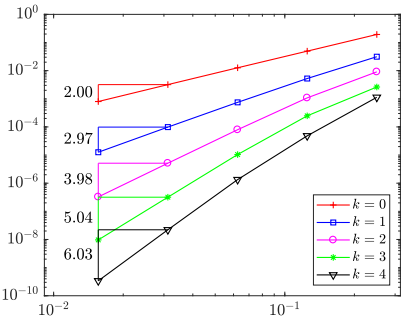

(e) Potential error, Refined meshes

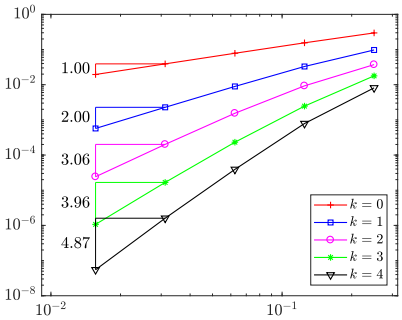

(f) Flux error, Refined meshes

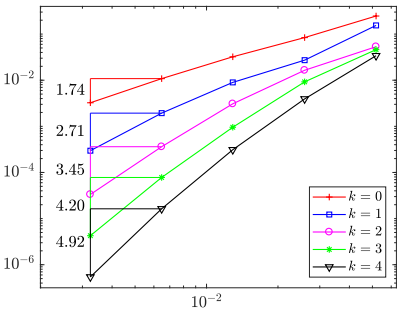

(g) Potential error, Hexagonal meshes

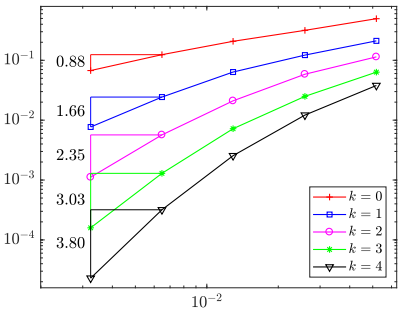

(h) Flux error, Hexagonal meshes

Figure 4: Rates of convergence of potential and flux errors, considering each one of the four triangulations (Example 3).

Table 1: History of convergence of L^2-norm of the Potential error, for each one of the four triangulations and $k \in \{0, 1, 2, 3\}$ (Example 1).

Triangles								
	$k=0$		$k=1$		$k=2$		$k=3$	
h	error	rate	error	rate	error	rate	error	rate
3.07e-02	1.23e-01		1.93e-02		1.69e-03		1.05e-04	
1.54e-02	2.95e-02	2.065	2.43e-03	2.999	1.05e-04	4.034	3.24e-06	5.036
7.68e-03	7.32e-03	2.005	3.06e-04	2.982	6.49e-06	3.995	1.01e-07	4.991
3.84e-03	1.82e-03	2.004	3.83e-05	2.997	4.04e-07	4.005	3.13e-09	5.006
1.92e-03	4.56e-04	2.001	4.79e-06	2.999	2.52e-08	4.003	9.77e-11	5.003

Cartesian								
	$k=0$		$k=1$		$k=2$		$k=3$	
h	error	rate	error	rate	error	rate	error	rate
6.25e-02	2.07e-01		5.13e-02		8.47e-03		8.41e-04	
3.12e-02	5.15e-02	2.004	6.44e-03	2.987	5.41e-04	3.959	2.79e-05	4.903
1.56e-02	1.29e-02	2.002	7.97e-04	3.015	3.40e-05	3.992	8.91e-07	4.969
7.81e-03	3.21e-03	2.004	9.92e-05	3.013	2.13e-06	4.005	2.81e-08	4.996
3.91e-03	8.03e-04	2.004	1.24e-05	3.008	1.33e-07	4.007	8.82e-10	5.003
1.95e-03	2.01e-04	1.993	1.55e-06	2.990	8.32e-09	3.985	2.77e-11	4.975

Refined								
	$k=0$		$k=1$		$k=2$		$k=3$	
h	error	rate	error	rate	error	rate	error	rate
2.50e-01	1.65e-01		4.39e-02		7.15e-03		6.79e-04	
1.25e-01	4.82e-02	1.773	5.62e-03	2.964	4.66e-04	3.940	2.34e-05	4.861
6.25e-02	1.30e-02	1.890	6.96e-04	3.014	2.94e-05	3.986	7.59e-07	4.944
3.12e-02	3.37e-03	1.943	8.63e-05	3.004	1.84e-06	3.987	2.41e-08	4.963
1.56e-02	8.57e-04	1.975	1.08e-05	3.005	1.15e-07	3.999	7.60e-10	4.988

Hexagonal								
	$k=0$		$k=1$		$k=2$		$k=3$	
h	error	rate	error	rate	error	rate	error	rate
5.18e-02	1.70e-01		4.43e-02		4.63e-03		3.81e-04	
2.59e-02	4.21e-02	2.013	6.22e-03	2.832	3.17e-04	3.872	1.31e-05	4.866
1.29e-02	1.07e-02	1.965	8.16e-04	2.915	2.05e-05	3.927	4.24e-07	4.917
6.47e-03	2.70e-03	1.996	1.04e-04	2.984	1.30e-06	3.995	1.35e-08	4.997
3.24e-03	6.77e-04	1.999	1.31e-05	2.993	8.20e-08	3.998	4.25e-10	4.999

Table 2: History of convergence of L^2-norm of the Flux error, for each one of the four triangulations, and $k \in \{0, 1, 2, 3\}$ (Example 1).

Triangles								
	$k=0$		$k=1$		$k=2$		$k=3$	
h	error	rate	error	rate	error	rate	error	rate
3.07e-02	2.38e-01		2.42e-02		1.67e-03		1.01e-04	
1.54e-02	1.19e-01	1.003	6.02e-03	2.013	2.18e-04	2.954	6.98e-06	3.874
7.68e-03	5.96e-02	0.998	1.50e-03	1.995	2.75e-05	2.973	4.56e-07	3.921
3.84e-03	2.98e-02	1.001	3.76e-04	2.001	3.45e-06	2.995	2.91e-08	3.970
1.92e-03	1.49e-02	1.001	9.39e-05	2.000	4.31e-07	2.998	1.84e-09	3.986

Cartesian								
	$k=0$		$k=1$		$k=2$		$k=3$	
h	error	rate	error	rate	error	rate	error	rate
6.25e-02	3.17e-01		6.18e-02		7.60e-03		7.44e-04	
3.12e-02	1.60e-01	0.986	1.54e-02	1.996	9.58e-04	2.980	4.71e-05	3.972
1.56e-02	8.01e-02	0.997	3.83e-03	2.013	1.20e-04	2.998	2.95e-06	3.996
7.81e-03	4.01e-02	1.001	9.52e-04	2.010	1.50e-05	3.005	1.85e-07	4.006
3.91e-03	2.00e-02	1.002	2.38e-04	2.006	1.88e-06	3.005	1.16e-08	4.007
1.95e-03	1.00e-02	0.996	5.94e-05	1.993	2.34e-07	2.989	7.22e-10	3.985

Refined								
	$k=0$		$k=1$		$k=2$		$k=3$	
h	error	rate	error	rate	error	rate	error	rate
2.50e-01	2.84e-01		5.37e-02		6.61e-03		6.57e-04	
1.25e-01	1.43e-01	0.990	1.35e-02	1.991	8.32e-04	2.990	4.11e-05	3.998
6.25e-02	7.15e-02	0.999	3.36e-03	2.009	1.04e-04	2.999	2.57e-06	4.002
3.12e-02	3.58e-02	0.997	8.34e-04	2.004	1.30e-05	2.993	1.60e-07	3.992
1.56e-02	1.79e-02	1.000	2.08e-04	2.004	1.63e-06	3.000	1.00e-08	4.001

Hexagonal								
	$k=0$		$k=1$		$k=2$		$k=3$	
h	error	rate	error	rate	error	rate	error	rate
5.18e-02	3.36e-01		4.75e-02		4.90e-03		3.41e-04	
2.59e-02	1.67e-01	1.007	1.21e-02	1.967	6.45e-04	2.926	2.22e-05	3.937
1.29e-02	8.24e-02	1.014	3.06e-03	1.977	8.23e-05	2.954	1.41e-06	3.953
6.47e-03	4.08e-02	1.021	7.68e-04	2.003	1.04e-05	3.000	8.91e-08	4.006
3.24e-03	2.02e-02	1.013	1.92e-04	2.002	1.30e-06	3.001	5.59e-09	4.003

Table 3: History of convergence of L^2-norm of the potential error, for each one of the four triangulations, and $k \in \{0, 1, 2, 3\}$ (Example 2).

Triangles								
	$k=0$		$k=1$		$k=2$		$k=3$	
h	error	rate	error	rate	error	rate	error	rate
3.07e-02	7.69e-01		2.25e-02		1.66e-03		1.00e-04	
1.54e-02	2.46e-01	1.652	3.24e-03	2.809	1.20e-04	3.812	3.67e-06	4.790
7.68e-03	6.89e-02	1.829	4.29e-04	2.905	8.06e-06	3.877	1.23e-07	4.877
3.84e-03	1.80e-02	1.938	5.51e-05	2.959	5.23e-07	3.946	4.00e-09	4.948
1.92e-03	4.57e-03	1.977	6.99e-06	2.980	3.33e-08	3.973	1.27e-10	4.974

Cartesian								
	$k=0$		$k=1$		$k=2$		$k=3$	
h	error	rate	error	rate	error	rate	error	rate
3.12e-02	3.22e-01		8.58e-03		5.97e-04		2.92e-05	
1.56e-02	9.95e-02	1.696	1.10e-03	2.960	4.12e-05	3.857	1.01e-06	4.862
7.81e-03	2.72e-02	1.872	1.41e-04	2.974	2.72e-06	3.930	3.30e-08	4.939
3.91e-03	7.06e-03	1.952	1.79e-05	2.982	1.74e-07	3.969	1.06e-09	4.974
1.95e-03	1.79e-03	1.972	2.26e-06	2.975	1.10e-08	3.966	3.36e-11	4.958

Refined								
	$k=0$		$k=1$		$k=2$		$k=3$	
h	error	rate	error	rate	error	rate	error	rate
2.50e-01	5.96e-01		5.84e-02		6.74e-03		7.11e-04	
1.25e-01	2.03e-01	1.552	7.66e-03	2.930	5.04e-04	3.740	2.68e-05	4.732
6.25e-02	5.70e-02	1.836	9.65e-04	2.988	3.44e-05	3.873	9.18e-07	4.864
3.12e-02	1.49e-02	1.934	1.23e-04	2.964	2.24e-06	3.930	3.01e-08	4.921
1.56e-02	3.78e-03	1.974	1.57e-05	2.975	1.43e-07	3.971	9.62e-10	4.966

Hexagonal								
	$k=0$		$k=1$		$k=2$		$k=3$	
h	error	rate	error	rate	error	rate	error	rate
5.18e-02	7.34e-01		4.08e-02		3.92e-03		2.90e-04	
2.59e-02	2.41e-01	1.610	5.91e-03	2.790	2.83e-04	3.791	1.08e-05	4.743
1.29e-02	7.33e-02	1.704	7.75e-04	2.914	1.91e-05	3.873	3.71e-07	4.842
6.47e-03	1.99e-02	1.887	9.93e-05	2.978	1.24e-06	3.961	1.21e-08	4.956
3.24e-03	5.13e-03	1.963	1.26e-05	2.989	7.90e-08	3.979	3.88e-10	4.978

Table 4: History of convergence of L^2-norm of the flux error, for each one of the four triangulations, and $k \in \{0, 1, 2, 3\}$ (Example 2).

Triangles								
	$k=0$		$k=1$		$k=2$		$k=3$	
h	error	rate	error	rate	error	rate	error	rate
3.07e-02	3.97e-01		2.80e-02		2.04e-03		1.16e-04	
1.54e-02	2.13e-01	0.902	7.05e-03	2.002	2.63e-04	2.970	7.30e-06	4.013
7.68e-03	1.09e-01	0.968	1.77e-03	1.989	3.34e-05	2.966	4.61e-07	3.970
3.84e-03	5.46e-02	0.993	4.42e-04	1.997	4.21e-06	2.989	2.90e-08	3.992
1.92e-03	2.73e-02	0.999	1.11e-04	1.998	5.28e-07	2.995	1.82e-09	3.995

Cartesian								
	$k=0$		$k=1$		$k=2$		$k=3$	
h	error	rate	error	rate	error	rate	error	rate
3.12e-02	1.76e-01		1.68e-02		1.08e-03		4.91e-05	
1.56e-02	8.84e-02	0.996	4.14e-03	2.025	1.34e-04	3.022	3.09e-06	3.991
7.81e-03	4.42e-02	1.001	1.03e-03	2.016	1.66e-05	3.014	1.93e-07	4.005
3.91e-03	2.21e-02	1.002	2.56e-04	2.008	2.07e-06	3.008	1.21e-08	4.006
1.95e-03	1.11e-02	0.996	6.39e-05	1.994	2.59e-07	2.990	7.56e-10	3.984

Refined								
	$k=0$		$k=1$		$k=2$		$k=3$	
h	error	rate	error	rate	error	rate	error	rate
2.50e-01	3.34e-01		6.69e-02		8.25e-03		7.53e-04	
1.25e-01	1.69e-01	0.982	1.65e-02	2.019	1.03e-03	3.009	4.77e-05	3.982
6.25e-02	8.50e-02	0.995	4.05e-03	2.026	1.27e-04	3.017	2.99e-06	3.996
3.12e-02	4.25e-02	0.997	1.00e-03	2.008	1.58e-05	3.000	1.87e-07	3.990
1.56e-02	2.12e-02	1.000	2.50e-04	2.004	1.97e-06	3.002	1.17e-08	3.999

Hexagonal								
	$k=0$		$k=1$		$k=2$		$k=3$	
h	error	rate	error	rate	error	rate	error	rate
5.18e-02	3.76e-01		5.06e-02		5.20e-03		3.63e-04	
2.59e-02	1.88e-01	0.999	1.29e-02	1.970	6.88e-04	2.919	2.34e-05	3.953
1.29e-02	9.18e-02	1.030	3.25e-03	1.978	8.76e-05	2.956	1.49e-06	3.951
6.47e-03	4.51e-02	1.030	8.15e-04	2.006	1.10e-05	3.001	9.42e-08	4.004
3.24e-03	2.23e-02	1.016	2.04e-04	2.003	1.39e-06	3.001	5.92e-09	4.002

Table 5: History of convergence of L^2-norm of the potential error, for each one of the four triangulations, and $k \in \{0, 1, 2, 3\}$ (Example 3).

Triangles								
	$k=0$		$k=1$		$k=2$		$k=3$	
h	error	rate	error	rate	error	rate	error	rate
3.07e-02	3.35e-01		1.69e-01		6.49e-02		4.83e-02	
1.54e-02	1.17e-01	1.522	2.42e-02	2.813	1.57e-02	2.056	8.80e-03	2.468
7.68e-03	3.52e-02	1.727	6.55e-03	1.881	2.65e-03	2.558	7.10e-04	3.617
3.84e-03	9.32e-03	1.918	1.23e-03	2.411	2.17e-04	3.607	3.12e-05	4.508
1.92e-03	2.41e-03	1.953	1.53e-04	3.007	1.44e-05	3.915	1.10e-06	4.828

Cartesian								
	$k=0$		$k=1$		$k=2$		$k=3$	
h	error	rate	error	rate	error	rate	error	rate
6.25e-02	8.11e-01		4.34e-01		1.97e-01		1.25e-01	
3.12e-02	2.79e-01	1.538	1.05e-01	2.043	3.79e-02	2.369	1.97e-02	2.655
1.56e-02	8.57e-02	1.699	2.33e-02	2.173	8.09e-03	2.229	2.50e-03	2.982
7.81e-03	2.49e-02	1.790	4.10e-03	2.509	1.04e-03	2.971	2.46e-04	3.350
3.91e-03	6.65e-03	1.906	5.94e-04	2.792	7.70e-05	3.756	1.04e-05	4.574
1.95e-03	1.70e-03	1.962	7.85e-05	2.910	4.96e-06	3.941	3.17e-07	5.018

Refined								
	$k=0$		$k=1$		$k=2$		$k=3$	
h	error	rate	error	rate	error	rate	error	rate
2.50e-01	1.93e-01		3.13e-02		9.06e-03		2.62e-03	
1.25e-01	4.93e-02	1.969	5.25e-03	2.575	1.08e-03	3.074	2.48e-04	3.404
6.25e-02	1.26e-02	1.964	7.46e-04	2.813	7.95e-05	3.758	1.04e-05	4.569
3.12e-02	3.19e-03	1.983	9.85e-05	2.914	5.13e-06	3.945	3.18e-07	5.024
1.56e-02	7.99e-04	1.996	1.26e-05	2.969	3.25e-07	3.981	9.65e-09	5.042

Hexagonal								
	$k=0$		$k=1$		$k=2$		$k=3$	
h	error	rate	error	rate	error	rate	error	rate
5.18e-02	2.46e-01		1.54e-01		5.33e-02		4.60e-02	
2.59e-02	8.40e-02	1.553	2.72e-02	2.503	1.64e-02	1.697	9.21e-03	2.321
1.29e-02	3.22e-02	1.376	8.97e-03	1.592	3.08e-03	2.402	9.56e-04	3.251
6.47e-03	1.08e-02	1.580	1.93e-03	2.224	3.62e-04	3.104	7.79e-05	3.633
3.24e-03	3.24e-03	1.742	2.96e-04	2.712	3.33e-05	3.447	4.26e-06	4.203

Table 6: History of convergence of L^2-norm of the flux error, for each one of the four triangulations, and $k \in \{0, 1, 2, 3\}$ (Example 3).

Triangles								
	$k=0$		$k=1$		$k=2$		$k=3$	
h	error	rate	error	rate	error	rate	error	rate
3.07e-02	4.70e-01		1.87e-01		1.18e-01		8.50e-02	
1.54e-02	2.73e-01	0.788	9.94e-02	0.918	5.24e-02	1.181	2.31e-02	1.889
7.68e-03	1.71e-01	0.672	5.12e-02	0.952	1.21e-02	2.107	3.24e-03	2.823
3.84e-03	9.79e-02	0.804	1.70e-02	1.592	2.28e-03	2.407	3.95e-04	3.036
1.92e-03	5.02e-02	0.965	4.36e-03	1.961	3.93e-04	2.537	3.92e-05	3.331

Cartesian								
	$k=0$		$k=1$		$k=2$		$k=3$	
h	error	rate	error	rate	error	rate	error	rate
6.25e-02	7.96e-01		3.33e-01		2.08e-01		1.56e-01	
3.12e-02	4.49e-01	0.823	1.63e-01	1.029	1.01e-01	1.040	6.89e-02	1.181
1.56e-02	2.47e-01	0.864	8.85e-02	0.881	3.62e-02	1.479	1.77e-02	1.961
7.81e-03	1.31e-01	0.911	3.13e-02	1.502	9.19e-03	1.981	2.46e-03	2.854
3.91e-03	6.68e-02	0.977	8.56e-03	1.874	1.53e-03	2.587	2.32e-04	3.413
1.95e-03	3.34e-02	0.997	2.19e-03	1.959	2.00e-04	2.928	1.66e-05	3.784

Refined								
	$k=0$		$k=1$		$k=2$		$k=3$	
h	error	rate	error	rate	error	rate	error	rate
2.50e-01	2.97e-01		9.71e-02		3.73e-02		1.78e-02	
1.25e-01	1.55e-01	0.936	3.30e-02	1.559	9.28e-03	2.007	2.46e-03	2.857
6.25e-02	7.83e-02	0.986	8.93e-03	1.884	1.54e-03	2.588	2.32e-04	3.408
3.12e-02	3.91e-02	1.000	2.28e-03	1.967	2.01e-04	2.933	1.67e-05	3.790
1.56e-02	1.95e-02	1.003	5.71e-04	1.996	2.42e-05	3.056	1.07e-06	3.963

Hexagonal								
	$k=0$		$k=1$		$k=2$		$k=3$	
h	error	rate	error	rate	error	rate	error	rate
5.18e-02	4.95e-01		2.11e-01		1.14e-01		6.34e-02	
2.59e-02	3.16e-01	0.647	1.22e-01	0.790	5.85e-02	0.964	2.50e-02	1.344
1.29e-02	2.07e-01	0.604	6.36e-02	0.934	2.10e-02	1.468	7.20e-03	1.785
6.47e-03	1.24e-01	0.745	2.43e-02	1.395	5.67e-03	1.899	1.29e-03	2.488
3.24e-03	6.74e-02	0.883	7.69e-03	1.664	1.12e-03	2.351	1.59e-04	3.029

Centro de Investigación en Ingeniería Matemática (CI^{2}MA)

PRE-PUBLICACIONES 2018 - 2019

2018-47 Marcelo Cavalcanti, Wellington Correa, André Domingos, Zaid Hajjej, Mauricio Sepúlveda, Rodrigo Véjar: *Uniform decay rates for a suspension bridge with locally distributed nonlinear damping*

2018-48 Gabriel N. Gatica, Cristian Inzunza: *An augmented fully-mixed finite element method for a coupled flow-transport problem*

2018-49 Sergio Caucao, Gabriel N. Gatica, Felipe Sandoval: *A fully-mixed finite element method for the coupling of the Navier-Stokes and Darcy-Forchheimer equations*

2018-50 Nicolas Barnafi, Gabriel N. Gatica, Daniel E. Hurtado, Willian Miranda, Ricardo Ruiz-Baier: *A posteriori error estimates for primal and mixed finite element approximations of the deformable image registration problem*

2018-51 Rodolfo Araya, Ramiro Rebolledo, Frederic Valentin: *On a multiscale a posteriori error estimator for the Stokes and Brinkman equations*

2018-52 Felisia A. Chiarello, Paola Goatin, Luis M. Villada: *Lagrangian-antidiffusive remap schemes for non-local multi-class traffic flow models*

2019-01 Paulo Amorim, Bruno Telch, Luis M. Villada: *A reaction-diffusion predator-prey model with pursuit, evasion, and nonlocal sensing*

2019-02 Ana Alonso-Rodriguez, Jessika Camaño, Eduardo De Los Santos, Rodolfo Rodríguez: *Divergence-free finite elements for the numerical solution of a hydroelastic vibration problem*

2019-03 Raimund Bürger, Daniel Inzunza, Pep Mulet, Luis M. Villada: *Implicit-explicit methods for a class of nonlinear nonlocal gradient flow equations modelling collective behaviour*

2019-04 Eligio Colmenares, Gabriel N. Gatica, Sebastian Moraga: *A Banach spaces-based analysis of a new fully-mixed finite element method for the Boussinesq problem*

2019-05 Antoine J. Cerfon, Tonatiuh Sanchez-Vizuet, Manuel Solano: *Adaptive Hybridizable Discontinuous Galerkin discretization of the Grad-Shafranov equation by extension from polygonal subdomains*

2019-06 Rommel Bustinza, Jonathan Munguia: *An HHO formulation for a Neumann problem on general meshes*

Para obtener copias de las Pre-Publicaciones, escribir o llamar a: Director, Centro de Investigación en Ingeniería Matemática, Universidad de Concepción, Casilla 160-C, Concepción, Chile, Tel.: 41-2661324, o bien, visitar la página web del centro: http://www.ci2ma.udec.cl







Centro de Investigación en
Ingeniería Matemática (CI²MA)
Universidad de Concepción

Casilla 160-C, Concepción, Chile
Tel.: 56-41-2661324/2661554/2661316
http://www.ci2ma.udec.cl